MULTISCALE MODELLING OF MASONRY STRUCTURES

A DISSERTATION

submitted in partial fulfillment of the

requirements for the award of the degree

of

MASTER OF TECHNOLOGY

in

EARTHQUAKE ENGINEERING

(With Specialization in Structural Dynamics)

by

DEVAYAN BHATTACHARJEE

(16526009)

DEPARTMENT OF EARTHQUAKE ENGINEERING

INDIAN INSTITUTE OF TECHNOLOGY ROORKEE

ROORKEE- 247 667 (INDIA)

MAY, 2018

CANDIDATE'S DECLARATION

I hereby declare that the study which is being presented in this Dissertation entitled "**MULTISCALE MODELLING OF MASONRY STRUCTURES**", submitted in the partial fulfillment of the requirements for the award of the degree of Master of Technology in Earthquake Engineering with specialization in Structural Dynamics, Indian Institute of Technology Roorkee, is an authentic record of my own work carried out for a period from June 2017 to May 2018, under the supervision of **Dr. Yogendra Singh**, Professor, Department of Earthquake Engineering, Indian Institute of Technology, Roorkee. The matter embodied in this dissertation work has not been submitted by me for the award of any other degree or diploma.

Date: **(DEVAYAN BHATTACHARJEE)**

Place: Roorkee

CERTIFICATE

This is to certify that the above statement made by the candidate is correct to the best of my knowledge.

Date: (**Dr. Yogendra Singh)**

Place: Roorkee

Professor and Head

Department of Earthquake Engineering

Indian Institute of Technology, Roorkee

Roorkee (Uttarakhand)-247667

India

ABSTRACT

Unreinforced masonry (URM) is one of the primogenital and most broadly used building material in the history of menfolk. There is a large number of URM buildings in the Indian subcontinent, most of which have not been premeditated for seismic loads. Recent Earthquakes have uncovered the seismic susceptibility of these URM buildings. The masonry piers of URM buildings are generally strong enough to bear the compressive forces, but weak in bending tension and in-plane shear. They are also very weak in out-of-plane bending.

In this thesis an extensive study of numerical modelling of masonry components is performed. Both FE modelling for a detailed analysis and EFM modelling for a more global analysis has been performed. The FE model is first attempted to be validated before being used to analyze a building model. The validation attempt is made by modelling the small scale tests. The EFM model is also used to model the masonry building. In EFM model the acceptance criteria to model the building in SAP2000 is done using ASCE 41(2017). The FE model is used model both the URM specimens and the retrofitted specimens. Attempt is made to observe whether the EFM method can accurately predict the URM behavior or not as it requires less computational resources.

ACKNOWLEDGEMENT

It is my great pleasure to express my most sincere gratitude and thankfulness to **Dr.Yogendra Singh**, Professor, Department of Earthquake Engineering, Indian Institute of Technology, Roorkee for his dedicated guidance, generous help and the precious time he gave in supervising this Seminar Report.

I would also sincerely thank all of my fellow friends and the staff of Department of Earthquake Engineering Department IIT Roorkee, who have helped me in every possible way in the successful completion of my seminar report.

I also take this occasion to thank my family for their help and encouragement in preparing this seminar report.

Place: IIT Roorkee Devayan Bhattacharjee

Date: (Enrolment No. 16526009)

TABLE OF CONTENTS

LIST OF FIGURES

LIST OF TABLES

Chapter 1

Introduction

1.1 GENERAL

URM has been one of the most popular building materials historically. It was used extensively until the usage of materials like timber, steel and wood became common (Abrams 2001). Even now in developing nations like India URM is still used for most of the constructions. In seismically prone areas URM has been observed to behave poorly. Such poor performance has led to major economic loss and also caused loss to human life. Some examples are the Kashmir earthquake of 2005, the Bhuj earthquake of 2001.

1.2 URM BEHAVIOR

URM has complex behavior. It is made up of two units viz. brick and mortar. Due to variability in the creation of brick specimens and in the quality of mortar the behavior of URM varies a lot from region to region. Even in the same country like India the brick may have different strength considering where it was made for example Sarangapani et al (2002) showed that bricks in northern India have better strength than bricks in southern India. Despite its widespread use URM is still considered a "non-engineered material" due to a lack of understanding of its behavior.

URM is considered as an anisotropic material as it consists of two units brick and mortar. It has adequate compressive strength but low tensile strength. URM consists of certain planes of weakness called "joints". It has two types of joints viz. the bed joint and the head joint. Bed joint is parallel to the brick face and head joint is perpendicular to the brick surface. It is considered that masonry is weaker when load is applied parallel to the bed joint that is along the direction of the head joint.

The choice of a suitable overstrength ratio (OSR) for masonry buildings has been confirmed by Paolo et al. (2008). Paolo et al. (2008) also stated that due to the high inconsistency in OSR, the choice of a single conservative value of OSR for an assumed building type does not entirely overcome the inherent confines of a linear analysis. They have recommended two

novel linear design procedures to solve the problem of the high inconsistency of OSR in masonry structures. The first method is a based on conventional linear elastic analysis followed by an appropriate redistribution of the shear force and bending moments. The second method consists of an initial approximation of the distribution of the internal forces founded on the strength of the masonry piers. OSR can be estimated through nonlinear numerical simulations and through experimentation on building models. OSR is expected to depend on a number of factors mostly related to modelling hypotheses. Therefore estimation of OSR cannot be done through experimentation alone it needs to be followed by up a numerical study as well. In a numerical study conducted by Morandi et al. (2006) the OSR was found to vary between 1.2 to 3.8 for two and three storey URM buildings with RC ring beams.

1.3 IN-PLANE ACTION

In in-plane direction, URM consists of five primary actions: (ASCE 41-2017)

a) *Deformation controlled actions*

i)Rocking

ii) Bed joint sliding

b) *Force controlled actions*

i) Toe crushing

ii) Diagonal tension

iii) Vertical compression

Past earthquakes show that the primary mode of failure under in-plane action is shear failure i.e. bed joint sliding failure. Tests conducted by Magenes and Calvi (1994), Epperson and Abrams (1989) and König et al. (1988), Zilch et al. (2002), Anthoine et al. (1994) and Abrams and Shah (1992) show that the axial load level play a vital role in both the type of cracking and post-cracking behavior of URM walls. A higher value of axial load caused an increase in strength was in terms of maximum horizontal load-carrying capacity, but worsened the seismic behavior as regards to ductility. Additionally, it was shown that the

transition from one mode of failure to another mode of failure could be obtained by altering normal force and/or mortar strength. Also a noteworthy consequence of the failure mechanism on post-cracking behavior was stated. The specimens that failed in rocking withstood displacements that were greater than the cracking displacements by several orders of magnitude even after multiple rocking cycles. Moreover, Abrams and Shah (1992) and Epperson and Abrams (1989) settled that the lateral strength of URM structures may be supposed to be the sum of the strength of all discrete URM walls rather than being equal to the strength of the weakest wall.

1.4 OUT-OF-PLANE ACTION

URM walls are very weak in out-of-plane action and need to be supported by cross-walls to counterattack the inertia forces caused by seismic action. In out-of-plane behavior the primary mode of failure of URM wall is bending. This out-of-plane bending leads to development of tensile stresses outside the capacity of URM walls and results in their failure. This out-of-plane failure of URM walls has been predominant in case of buildings with high ceilings and long walls and with flexible floors/roof. Out-of-plane failure is the most serious life-safety hazard for masonry construction (Yi 2002). The susceptibility of masonry walls towards out-of-plane behavior is linked to their mode of construction which involves stacking of rows of bricks one over the other and held together by mortar. The exact intricacy is related with the exceedingly non-linear masonry behavior, mostly ruled by cracking and instability rather than usual material failure (Yi 2002). Parameters influencing the failure modes of a URM wall exposed to out-of-plane loads are the sizes of the wall, slenderness, boundary conditions, the relative resistance of the bricks and the mortar joints, the ratio applied loads/dead loads and in the case of seismic loads the peak velocity demand at the base and the top of the wall (Elmenshawi et Al., 2010; Griffith et Al., 2005). Most URM walls existing in buildings are supported on three or four sides. These boundary conditions lead to the consideration of these walls being subjected to bi-axial bending when subjected to out-of-plane loads. Therefore, the wall endures a grouping of horizontal, vertical and diagonal bending (Vaculik 2010) that have to be taken into account. Under out-of-plane loads, URM walls undergo either line failure or stepped failure. In case of weak bricks and

strong mortar, line failure tends to occur and in case of strong bricks and weak mortar, stepped failure tends to occur.

Figure 1.1 represents the in-plane and out-of-plane behavior in a typical masonry building. As can be seen in the diagram below; the piers between door and window openings are exposed to shear force and bending moment caused by lateral loads and are the most crucial mechanisms for counterattacking in-plane forces. The stresses in these piers are greater than the portion of the wall above and below the openings, and can cause failure when it exceeds the capacity under the combined action of axial force, bending moment and shear force.

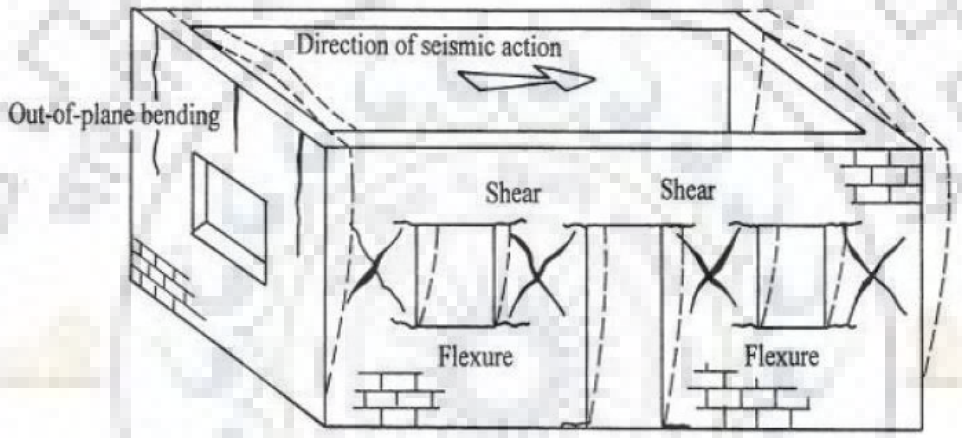

Figure 1.1 Representative modes of failure for a masonry building (Tomazevic 1999)

1.5 MODELLING TECHNIQUES

Modelling of masonry is a complex task due to its anisotropic nature. Masonry has predefined planes of weakness which consist of mortar which makes it difficult to model the masonry. Even after cracking at the mortar joints it can undergo large deformations and rotations as the behavior after cracking is governed by interaction of different blocks formed by cracking. This makes it a challenge to numerically model the masonry. Two popular approaches which are used nowadays to numerically model masonry to study the seismic behavior are the micro-modelling or continuum approach and the macro-modelling or discrete element modelling approach. The techniques used for micro-modelling approach are the Finite Element Method (FEM) and Distinct Element Method (DEM) while the techniques used for macro-modelling approach are the Pier Analysis Method (PAM) and the Equivalent

Frame Method (EFM). The micro-modelling approach is suitable to model at the component level as it is computationally demanding while the macro modelling approach is suitable to model the structure at the global level as it is less computationally demanding. The Finite Element Method has been widely used in the past to model the in-plane behavior of URM but its use in modelling the out-of-plane behavior of masonry is limited. The homogenized approach which considers the masonry as a continuum instead consisting of two units is not very successful in modelling the behavior of masonry. A few researchers also used the boundary element method to model the in-plane and out-of-plane behavior of masonry but the complexity resulting from a large number of interacting interfaces generated by the cracking of masonry makes it difficult to use this approach. The Distinct Element Method was developed due to the similarity of cracked masonry to jointed rock mass. It has proven to be an effective tool for the in-plane and out-of-plane modelling of masonry. Under both static and dynamic loads.

1.6 OBJECTIVES

The present study has been performed with the following objectives:

1. To numerically model the URM specimen both in in-plane and out-of-plane behavior and compare the results with the experimental results reported by Kadam (2015).

2. To numerically model the strengthened URM specimen both in in-plane and out-of-plane behavior and compare the results with the experimental results reported by Kadam (2015).

3. To numerically model the masonry half scale model in SAP2000 using Equivalent Frame Modelling method.

4. To numerically model the same masonry half scale model in ABAQUS using Concrete Damage Plasticity (CDP) model and compare the results with that of the model simulated in SAP2000.

1.7 METHODOLOGY AND SCOPE

The present study focusses on the numerical modelling of masonry components and a half scale model of masonry using two different approaches viz. micro-modelling and macro-modelling approach. First, the in-plane and out-of-plane behavior of masonry is simulated in

ABAQUS using the Concrete Damage Plasticity (CDP) model. The CDP model is used to simulate the nonlinearity of masonry. This model was developed initially for masonry but then it was demonstrated by many researchers to be applicable to masonry as well. The diagonal compression test is modelled to simulate the in-plane response and the four point bending test is modelled to simulate the out-of-plane response. The analysis results of ABAQUS are compared with the experimental values reported by Kadam (2015). A half scale masonry model tested by Kadam (2015) is then modelled in SAP2000 using Equivalent Frame Method(EFM) and the same model is also modelled in ABAQUS using the CDP model. The results obtained in both the softwares are then compared to study the differences observed in the analysis values. ASCE 41 (2017) and FEMA 356 (2000) guidelines have been used as acceptance criteria for modelling the half scale model using EFM. In-plane capacity of URM piers have been estimated as per Pasticier et al. (2008).

1.8 ORGANIZATION OF THESIS

Chapter-1 describes the behavior of URM, the in-plane and out-of-plane actions of URM, the modelling techniques used to numerically model masonry structures and the objectives and scope of the present study.

Chapter-2 consists of a state-of-the-art study of the earlier studies conducted to study the seismic behavior of masonry. It discusses the observations made in the past of the behavior of masonry under seismic action. It also discusses all the efforts made in the field of numerical modelling of masonry.

Chapter-3 discusses the Finite Element Modelling technique used in the present study to model the in-plane and out-of-plane experimental models. It discusses the material model called Concrete Damage Plasticity (CDP) which is used to simulate the masonry in the Finite Element software ABAQUS.

Chapter-4 discusses the technique called Equivalent Frame Modelling. It discusses the acceptance criteria and the concept of backbone curve.

Chapter-5 consists of the FE and EFM modelling of a half scale masonry model and a comparison of the results obtained in both the techniques.

Chapter-6 concludes the thesis and summarizes all the important observations made in the study.

Chapter 2

Literature Review

2.1 INTRODUCTION

URM is used as a common construction material in most of developing nations due to its availability and also due to the fact that it is a cheap building material. It is strong in resisting the in-plane forces but weak in resisting the out-of –plane forces. URM buildings mostly fail in in-in-plane shear and out-of-plane bending. This usually happens because URM has satisfactory compressive strength but low value of tensile strength. In this chapter, a literature review on the numerical studies conducted on the in-plane and out-of-plane behavior have been carried out.

2.2 NUMERICAL MODELLING

Masonry being constituted by two units viz. bricks and mortar is a difficult entity to model numerically. Its anisotropic property, arrangement of the brick layers and presence of predefined planes of weakness in the form of mortar joints adds on to its modelling complexity. The two main approaches to model the masonry have been the macro-modelling and the micro-modelling techniques.

In macro-modelling, the performance of URM walls is modelled by assuming a predefined mode of failure. In micro-modelling however, the mode of failure and the behavior of URM walls is obtained using numerical approaches such as Finite Element Method (FEM) or Discrete Element Method (DEM). This section presents a review of the available literature on the various macro and micro-modelling research carried out in the past by different researchers. Both research concerning in-plane and out-of-plane behavior has been reviewed.

2.2.1 Macro-modelling

Macro-modeling approach is favored to mimic the seismic performance of real size URM buildings, due to its ease and rational computational requirements. Two popular macro-

models that are used are the Pier Analysis Method (PAM) and the Equivalent Frame Method. PAM is a abridged technique of analyzing masonry buildings, in which masonry walls are supposed to contain dissimilar piers. The stiffness of each pier is calculated bearing in mind the end conditions; and the wall shear force is dispersed amongst different piers in percentage to their stiffness. This method of distributing base shear force amongst different piers has been used by Tomazevic (1999) for the nonlinear analysis of masonry buildings. In this procedure, the distinct piers are modelled as two-noded spring elements having multi-linear elastic properties, defined in the in-plane direction of the pier/wall. Spandrels connecting the piers are modeled as rigid frame elements.

Early efforts of macro-modelling of URM buildings were founded on 'Storey Mechanism' tactic (Tomazevic 1987). Mengi and McNiven (1989) considered the behavior of URM buildings using PAM, by modelling floors as rigid diaphragms, and assuming that the wall elements have shear strength only in their own plane. The nonlinear effect was considered by using equivalent linear method. Costley and Abrams (1995) later planned nonlinear static pushover analysis for the masonry structures. In this method, load is increased unceasingly until the structure touches a target displacement or collapses. At each load step, member stiffness is re-estimated to account for yielding and plasticity. Azam (2011) used this method for nonlinear modeling and performance evaluation of a masonry school building in Indian Himalayas, considering the modelling and acceptance criteria of FEMA 356 (2000).

PAM performs storey-by-storey analysis, bearing in mind the state of stress in vertical structural elements only; hence it is not precise enough to achieve global analysis of multistory buildings. To overcome these confines, equivalent frame modeling of masonry walls has been used by several researchers (Kappos et al., 2002; Salonikios et al., 2003; Pasticier et al, 2008 and Belmouden and Lestuzzi, 2009) for valuation of global behavior of masonry buildings. This technique gives good understanding about the inter-story displacements, strength of the building and global failure mechanism (Magenes and Fontana 1998; Magenes 2006). EFM had been successfully used in India by Prasad (2009); Prasad et al. (2009); Patil et al. (2010); Singh et al. (2012) in the past for susceptibility valuation of school and urban low-rise housing in Northern India. Salonikios et al. (2003) implemented nonlinear static (pushover) method for analysis of masonry buildings using EFM.

2.2.2 Micro-modelling

In micro-modelling tactic, a thorough analysis of stresses and strains is executed typically at constituent level. Micro-modelling tactic delivers a more thorough understanding of the behavior of masonry and is favored for identifying local crack pattern (Lotfi and Shing 1994; Lourenco and Rots 1997; Oliveira and Lourenco 2004; Binda et al. 2006; Chaimoon and Attard 2009). Its application however, is typically limited to constituent level due to huge computational resources essential for real size structures.

Dependent on the obligation of correctness in analysis, ease in approximation, and computation time essential, diverse levels of intricacies have been used in micro-modelling of masonry. The modelling tactic may be heterogeneous or homogenous depending on the analysis tool used. In heterogeneous modelling, masonry units and mortar are modelled distinctly. This approach suits for small size models, only. Because of the intricacy of modelling, the computational exertion required for a real size structure cannot be handled in sensible time. Consequently, the homogeneous modelling approach is more prevalent, in which the masonry units and mortar elements are presumed to be smeared and characterized by an isotropic or anisotropic material (Betti and Vignoli 2008; Zucchini and Lourenço 2002; Luciano and Sacco 1997; Mistler et al. 2007; Milani et al.2009; Kalali and Kabir 2010). In this approach, it is necessary to have test results of large masonry parts, which contain adequate unit and mortar combinations.

In micro modeling, Finite Element Method (FEM) and Discrete Element Method (DEM) are two encouraging tools to discover thorough behavior, viz. crack initiation and damage pattern. Usually, the models based on Finite Element (FE) formulation employ nonlinear damage constitutive models and friction models (Atmaturktur et al. 2010; Berto et al. 2004; Brasile et al. 2010; Dhanasekar and Haider 2008; Roca et al. 2010; Uva and Salerno 2006; Zienkiewicz et al. 2005) to simulate behavior of masonry. Numerous nonlinear material models have been advanced or altered to fit the masonry behaviour. Dhanasekar et al. (1985) modelled masonry as a continuum with middling properties. To define failure under biaxial stress, a 3D surface in terms of the two normal stresses and shear stress or the two principal stresses and their orientation to the bed joints is required. Syrmakezis and Asteris (2001) found that failure surface of anisotropic masonry material under biaxial stress has aptitude to

guarantee the closed shape. A 3D model of a masonry bridge has been analyzed by Fanning and Boothbay (2001) by means of Druckers Prager material model in ANSYS software. The bridge model was analyzed for service loads by including field testing results. The study tinted the need for more truthful tests on materials of bridge to achieve exactness in results.

Models based on Discrete Element (DE) originations have also been stated (Bretas et al. 2014; Lemos 2007; Masood 2006) to mimic the nonlinear behavior of masonry fruitfully. The Discrete Element Method (DEM) is a numerical method exactly intended to solve glitches where continuity cannot be guaranteed during the analysis. The method is proficient in analyzing system of numerous frames undergoing large dynamic or pseudo static absolute or relative motions. Dialer (1992) used DEM to analyze a small scale two brick specimen under the action of shear stress. Psycharis et al. (2000) used DEM to examine the steadiness of a free-standing column under seismic excitation using 2D model, abandoning the deformability of blocks and found DEM to be effective in mimicking the progressive collapse of block type structures. DEM was used by Zhuge (1998, 1999) to analyze the structural performance of URM using a stress boundary where the horizontal load was monotonically applied. However, the failure pattern and the principal stress distribution did not compare well with the experimental and finite element results. Later Zhuge and Hunt (2003) used DEM to mimic the response of URM shear wall wallettes with a new model substituting stress boundary with a gradually increasing displacement boundary. They analyzed URM shear wall wallettes with and without opening and found that the results related well with the results of experiment and finite element models (Lourenco 1996). Lemos (1995, 1998) demonstrated the application of DEM using 3DEC software code to evaluate the ultimate load carrying capacity of an old masonry arch bridge. Recently, Nakagawa et al. (2012) executed a shake-table test on 3m x 3m x 3m brick masonry model built with Pakistani bricks and simulated its behavior using Extended Distinct Element Method (EDEM). These simulated results were found to be in full covenant with results of the shake-table tests.

Giamundo et al. (2014) related different computational approaches of masonry modeling. They settled that FEM modeling approach is more dependable compared with DEM. As per their research for low unit strength masonry, the investigational behavior in terms of first

crack, trend, failure and smeared crack pattern can be efficaciously simulated using FEM. Contrariwise, the DEM model was not able to capture the investigational behavior.

2.3 SUMMARY

The literature on numerical modelling of masonry has been reviewed in this chapter. It is seen that the two most common approaches for modelling masonry are the macro-modelling and the micro-modelling approach. The macro-modelling being preferred where a large size structure is to be analyzed and the micro-modelling approach being used where a detailed analysis of a small structure is to be carried out. Some studies preferred using the EFM method over the PAM method to overcome its limitations. Also some comparative studies have been carried out comparing the macro-modelling and the micro-modelling approach. It has been found that for real life building the macro-modelling approach can sufficiently predict the results.

Chapter 3

FE Modelling

3.1 INTRODUCTION

Masonry is an anisotropic material. It consists of two units mortar and brick. Due to this heterogeneous nature modelling of masonry becomes a very complex task. Due to variability of quality and nature of mortar and changeability in the arrangement of brick units there results a huge number of possible groupings which add to the intricacy of analysis. The heterogeneity in between the bricks in the form of mortar create a discontinuum in the URM structure. These discontinuities act as predefined planes of weakness in the URM structure. Modelling of these discontinuities increase the difficulty of analysis.

3.2 APPROACHES

To numerically model a URM structure the most commonly used approaches are viz. micro-modelling approach and macro-modelling approach. The micro-modelling method is of two types viz. the heterogeneous micro-modelling method and the homogeneous micro-modelling method.

3.2.1 Macro-modelling approach

In the macro-modelling approach, the whole structure is venerated as a single component with lumped properties. This approach is ideal due to its simplicity and also when the structure to be analyzed is a big structure and the computational assets available are not suitable for a detailed analysis. This approach gives judiciously precise results.

3.2.2 Micro-modelling approach

3.2.2.1 Heterogeneous micro-modelling method

In this method, the stress analysis is conducted at the component level. It involves a detailed analysis of the URM structure considering the heterogeneity existing in the structure that is

the brick and mortar are considered as separate entities and both their properties are utilized while performing the analysis. It gives a more accurate result as compared to other approaches. The micro-modelling approach is ideal for identifying local crack pattern (Lotfi and Shing 1994; Lourenco and Rots 1997; Oliveira and Lourenco 2004; Binda et al. 2006; Chaimoon and Attard 2009). But this approach requires a lot of computational resource due to the complexity involved in modelling the heterogeneity existing in URM. As a result this approach is ideal only for analysis at the component level and in relatively small models.

3.2.2.2 Homogeneous micro-modelling method

In this method, the URM is idealized as a single entity. The brick and mortar are assumed to be smeared and represented by an isotropic or anisotropic material (Betti and Vignoli 2008; Zucchini and Lourenço 2002; Luciano and Sacco 1997; Mistler et al. 2007; Milani et al.2009; Kalali and Kabir 2010). This method requires test results of masonry parts comprising acceptable mortar and brick combinations. The homogenized micro-modelling method has been preferred to carry out the numerical modelling in this thesis as it is computationally simpler and gives results with an acceptable level of error.

The different tactics to model masonry were reported by Lourenco and Rots (1997) as shown in figure 3.1.

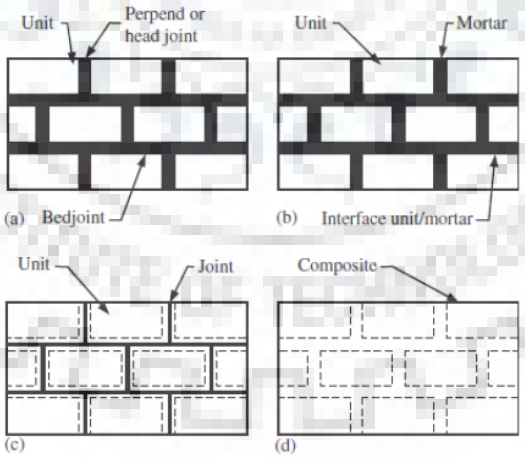

Figure 3.1 Tactics for modelling masonry: (a) Masonry Sample; (b) Detailed micro-modelling (discrete crack); (c) Simplified micro-modelling (discrete crack); (d) Micro-modelling (smeared crack) (Lourenco and Rots 1997)

In micro-modelling, Finite Element Method (FEM) and Discrete Element Method (DEM) are the two most widespread tools used to reconnoiter comprehensive performance viz. crack instigation and damage configuration. The models using FEM incorporate nonlinear damage constitutive models and friction models (Atmaturktur et al. 2010; Berto et al. 2004; Brasile et al. 2010; Dhanasekar and Haider 2008; Roca et al. 2010; Uva and Salerno 2006; Zienkiewicz et al. 2005) to mimic the behavior of masonry. Dhanasekar et al. (1985) modelled masonry as a continuum with average assets. To express failure under biaxial stress, a 3D surface in terms of the two normal stresses and shear stress (or the two principal stresses and their alignment to the bed joints) is essential. Syrmakezis and Asteris (2001) found that failure surface of anisotropic masonry material under biaxial stress has capability to ensure the closed figure. A 3D model of a masonry bridge has been investigated by Fanning and Boothbay (2001) using Druckers-Prager material model in ANSYS software. The bridge model was examined for service loads by integrating field testing outcomes. The study emphasized the need for more genuine tests on materials of bridge to attain precision in the outcomes.

Models grounded on Discrete Element (DE) interpretations have also been stated (Bretas et al. 2014; Lemos 2007; Masood 2006) to mimic the nonlinear performance of masonry with success. The Discrete Element Method (DEM) is a numerical practice explicitly intended to answer problems wherever continuity cannot be warranted all the way through the analysis. The method is adept at scrutinizing scheme of numerous bodies undergoing large dynamic or pseudo static absolute or relative motions. Dialer (1992) applied DEM to study a small scale two brick specimen under the action of shear stress. Psycharis et al. (2000) applied DEM to investigate the steadiness of a free standing column under seismic excitation by means of 2D model, disregarding the deformability of blocks and found DEM to be effectual in feigning progressive failure of block type structures. The DEM was applied by Zhuge (1998, 1999) to investigate the structural performance of URM using a stress limit where the horizontal load was monotonically applied. Yet, the failure array and the principal stress distribution did not match well with the experimental and finite element outcomes. Later Zhuge and Hunt (2003) applied DEM to mimic the reaction of URM shear wall wallettes with a new model substituting stress limit with a gradually accumulative displacement limit. They examined URM shear wall wallettes with and lacking opening and found that the results related well

with the results of experiment and finite element models (Lourenco 1996). Lemos (1995, 1998) demonstrated the application of DEM using 3DEC software code to evaluate the vital load carrying capacity of an old masonry arch bridge. Recently, Nakagawa et al. (2012) executed a shake-table test on 3m x 3m x 3m brick masonry model erected with Pakistani bricks and computer-generated its behaviour using Extended Distinct Element Method (EDEM). These simulated results were found to be in full covenant with outcomes of the shake-table examinations.

Giamundo et al. (2014) have compared dissimilar computational tactics of masonry modelling. They resolved that FEM modelling tactic is further dependable paralleled with DEM. As per their research for low unit strength masonry, the investigational performance in terms of first crack, trend, failure and smeared crack pattern can be positively computer-generated using FEM. On the other hand, the DEM model was not able to capture the investigational performance.

In current readings, concrete damage plasticity model has been used to characterize the nonlinear behavior of masonry and the damage in tension and compression is confirmed with investigational outcomes (Berto et al. 2004; Pelà et al. 2011; Sousa et al. 2013; Agnihotri et al. 2013; Choudhary et al. 2015). This model was initially established to mimic performance of brittle materials like concrete and rocks by bearing in mind two scalar variables which monitor damage under tension and compression (Faria et al. 1998; Lubliner et al. 1989). Numerous studies have been accomplished on standardization and endorsement of constitutive models for masonry (Fouchal et al. 2009; Barbosa et al. 2010; Vyas and Reddy 2010).

3.3 Concrete Damage Plasticity (CDP) Model

CDP model was advanced to capture the permanent effects of damage which arise in concrete under low confining pressure. Masonry also being a brittle material, its performance is identical to that of concrete. The subsequent features of material performance define the likeness between masonry and concrete (Faria et al. 1998; Lubliner et al. 1989; Berto et al. 2004; Pelà et al. 2011; Sousa et al. 2013):

- Dissimilar strengths in tension and compression.

- Softening comportment in tension as contrasting to preliminary hardening shadowed by
  softening in compression.
- Dissimilar degradation of the elastic stiffness in tension and compression.
- Stiffness retrieval effects throughout cyclic loading.
- Rate sensitivity, particularly a growth in the peak strength with strain rate.

CDP is a continuum, plasticity-based, damage model for concrete. It assumes that the main two failure mechanisms are tensile cracking and compressive crushing of the concrete material. The progress of the yield (or failure) surface is measured by two hardening variables, $\widetilde{\varepsilon_t^{pl}}$ and $\widetilde{\varepsilon_c^{pl}}$, associated with failure mechanisms under tension and compression loading, respectively. We refer to $\widetilde{\varepsilon_c^{pl}}$ and $\widetilde{\varepsilon_t^{pl}}$ as compressive and tensile equivalent plastic strains, individually. The model accepts that the uniaxial tensile and compressive response of concrete is categorized by damaged plasticity, as shown in figure 3.2

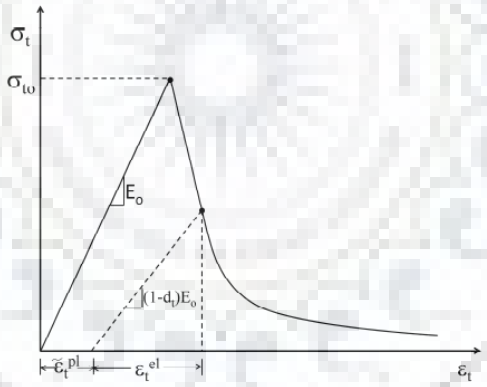

Figure 3.2 Behavior of concrete in uniaxial tension

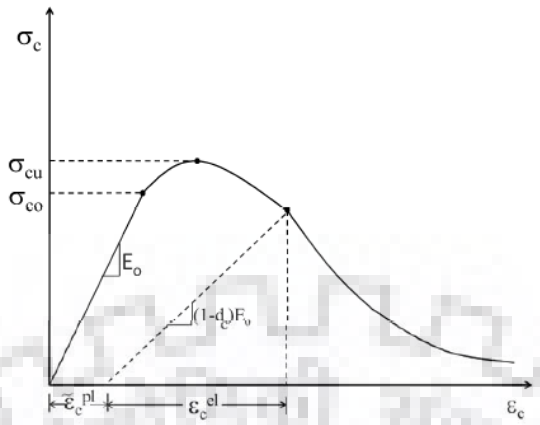

Figure 3.3 Behavior of concrete in uniaxial compression

In tension, the stress– strain retort of concrete (Figure 3.2) shadows a linear elastic affiliation, till the peak stress is reached. Then, micro-cracks start to spread in the material, an occurrence which is macroscopically characterized by softening in the stress-strain affiliation. In Figure 3.2, E_o signifies early uncracked modulus of elasticity conforming to peak tensile stress) (σ_{to}) . The total tensile strain (ε_t) has been expressed as elastic tensile strain (ε_t^{el}) and equivalent tensile plastic strain ($\widetilde{\varepsilon_t^{pl}}$)

Under axial compression, the response is linear till the value of yield stress is reached. In Figure 3.3, E_o characterizes initial uncracked modulus of elasticity conforming to the yield compressive stress (σ_{co}). The total compressive strain (ε_c) has been articulated as elastic compressive strain (ε_c^{el}) and equivalent compressive plastic strain ($\widetilde{\varepsilon_c^{pl}}$).

Beyond yield stress, the response is characteristically categorized by hardening, which expects compression crushing, embodied by a softening branch yonder the peak stress (σ_{cu}). When the specimen is unburdened from any point on the strain softening branch of the stress-strain curve, the unloading retort is detected to be weakened and the elastic stiffness of the material seems as if to be damaged (or degraded). The degraded retort of concrete is regarded by two autonomous uni-axial damage variables, d_c and d_t which are assumed to be functions of the plastic strains, temperature, and field variables:

$$d_t = d_t\,(\,\widetilde{\varepsilon_t^{pl}}, \theta, f_i\,); 0 \le d_t \le 1$$

$$d_c = d_c\left(\widetilde{\varepsilon}_c^{pl}, \theta, f_i\right); 0 \le d_c \le 1$$

If E_o is the initial (undamaged) elastic stiffness of the material, the stress-strain relations under uni-axial tension and compression loading are:

$$\sigma_t = (1 - d_t)\, E_0\, (\varepsilon_t - \widetilde{\varepsilon}_t^{pl})$$

$$\sigma_c = (1 - d_c)\, E_0\, (\varepsilon_c - \widetilde{\varepsilon}_c^{pl})$$

Under uni-axial loading, cracks spread in a route crosswise to the stress. The creation and spread of cracks cause a decrease in existing load-carrying extent, which in turn tips to surge in the effective stress. The effect is less distinct under compressive loading; yet, after a substantial quantity of crushing, the actual load-carrying area is significantly reduced. Thus effective uni-axial stresses, $\bar{\sigma}_c$ and $\bar{\sigma}_t$ are given as:

$$\bar{\sigma}_t = \frac{\sigma_t}{(1-d_t)} = E_0\, (\varepsilon_t - \widetilde{\varepsilon}_t^{pl})$$

$$\bar{\sigma}_c = \frac{\sigma_c}{(1-d_c)} = E_0\, (\varepsilon_c - \widetilde{\varepsilon}_c^{pl})$$

Total strain rate is governed by additive strain rate decomposition,

$$\dot{\varepsilon} = \dot{\varepsilon}^{el} + \dot{\varepsilon}^{pl}$$

Where, total strain rate is considered by $\dot{\varepsilon}$ and the superscripts '*el*' and '*pl*' signify the elastic and plastic influence of the strain rate, individually. The stress-strain relations are ruled by scalar damaged elasticity:

$$\sigma = D^{el}\, (\varepsilon - \varepsilon^{pl}) = (1\text{-d})\, D_0^{el}\, (\varepsilon - \varepsilon^{pl})$$

Where, D_o^{el} is the initial undamaged elastic stiffness of the material, $D_o^{el} = (1\text{-}d)\, D_o^{el}$ is the degraded elastic stiffness and *d* is the scalar stiffness degradation variable (for un-damaged material, $d = 0$, and for fully damaged material $d = 1$). Damage allied with the failure mechanisms of the concrete, then, outcomes in a decrease in the elastic stiffness.

In concrete damage plasticity theory, the stiffness degradation is isotropic and characterized by a single degradation variable, *d*. The effective stress is defined as,

$$\bar{\sigma}^{def} = D_0^{el} (\varepsilon - \varepsilon^{pl})$$

The Cauchy stress is linked to the effective stress by means of the scalar degradation relation,

$$\sigma = (1 - d)\, \bar{\sigma}$$

For any definite cross-section of the material, the factor (*1-d*) symbolizes the ratio of the real load carrying area to the whole section area. In the lack of damage (*d=0*) the effective stress $\bar{\sigma}$ is correspondent to the Cauchy stress (σ). As soon as damage ascends, the effective stress is auxiliary expressive than the Cauchy stress, as it is the real area that is counterattacking the external load. Thus, the plasticity complications are outlined in terms of effective stress. The degradation variable is ruled by a set of hardening variables, $\dot{\varepsilon^{pl}}$, besides the effective stress.

The hardening variables $\dot{\varepsilon_t^{el}}$ and $\dot{\varepsilon_c^{el}}$ are grounded on the uni-axial loading circumstances. Under uni-axial condition, the stress curves have the form:

$$\sigma_t = \sigma_t (\widetilde{\varepsilon_t^{pl}}, \dot{\widetilde{\varepsilon_t^{pl}}}, \theta, f_i)$$

$$\sigma_c = \sigma_c (\widetilde{\varepsilon_c^{pl}}, \dot{\widetilde{\varepsilon_c^{pl}}}, \theta, f_i)$$

where, the subscripts t and c refer to tension and compression, correspondingly; $\dot{\widetilde{\varepsilon_t^{pl}}}$ and $\dot{\widetilde{\varepsilon_c^{pl}}}$ are corresponding plastic strain rates, $\widetilde{\varepsilon_t^{pl}} = \int_0^t \dot{\widetilde{\varepsilon_t^{pl}}}\, dt$ and $\widetilde{\varepsilon_t^{pl}} = \int_0^t \dot{\widetilde{\varepsilon_c^{pl}}}\, dt$ are the corresponding plastic strain, θ is the temperature, and f_i, (i = 1,2....) are the additional predefined field variables.

3.4 VALIDATION USING SMALL SCALE TESTS

3.4.1 Material properties of masonry

The elementary material properties used for CDP modelling of masonry, have been taken from the actual laboratory tests conducted and reported by Kadam (2015). And values of a few selected constants which cannot be attained from direct measurements, have been referred from literature. The average value of compression strength and modulus of elasticity of masonry have been attained as 3.47 N/mm2 and 2184.35 N/mm2, individually from the compressive load tests on prisms (Table 2.2). Density of the masonry has been measured as

1920 kg/m3 from IS 875 Part I (IS 875 1987). The breaking load on specimens has been employed to compute the tensile strength (f_t) as per the procedure suggested in ASTM (ASTM 2010b). The average value of tensile strength of masonry is taken equal to the average value of modulus of rupture. The average value of tensile strength for bending perpendicular to bed joint is taken as 0.343N/mm^2 and the average value of tensile strength for bending parallel to bed joint is taken as 0.963 N/mm^2.

To generate the compressive stress-strain curve the procedure given by Kaushik et al. (2007) has been considered. Figure 3.4 shows the nature of the compressive curve given by Kaushik et al. (2007).

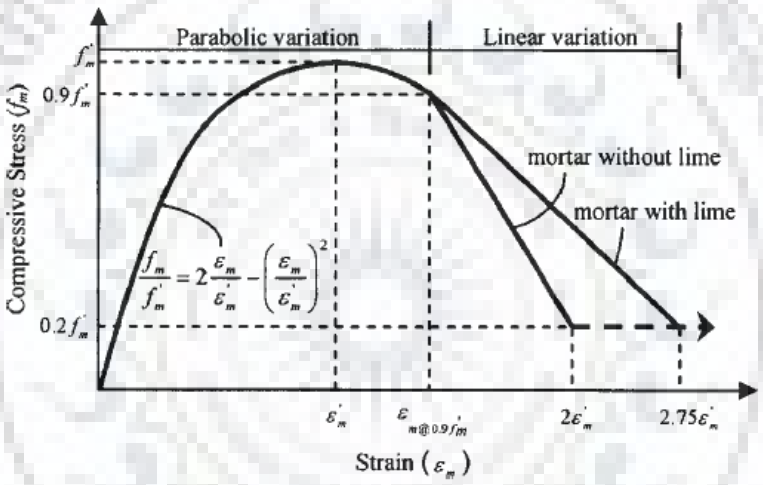

Figure 3.4 Stress-strain curve given by Kaushik et al. (2007)

To generate the stress-strain curve for masonry in tension the model given by Chen et al. (2008) has been used. The model is expressed as follows:

$$\sigma = \begin{Bmatrix} E_t \mathcal{E};\ \mathcal{E} < \mathcal{E}_t \\ K_r f_t;\ \mathcal{E} > \mathcal{E}_t \end{Bmatrix}$$

$$K_r = \left[1 + \left(C_1 \frac{\mathcal{E} - \mathcal{E}_t}{\mathcal{E}_v}\right)^3\right] e^{\left(-C_2 \frac{\mathcal{E} - \mathcal{E}_t}{\mathcal{E}_v}\right)} - \frac{\mathcal{E} - \mathcal{E}_t}{\mathcal{E}_v}\left(1 + C_1^3\right) e^{(-C_2)}$$

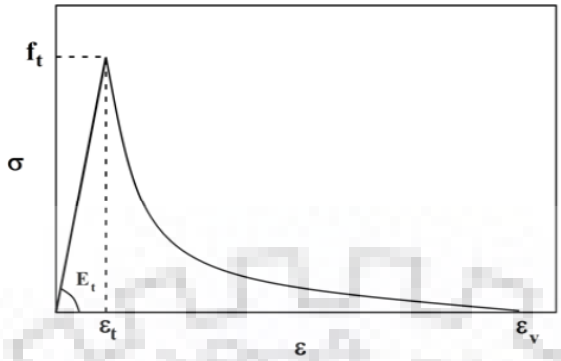

Figure 3.5 Stress-strain curve given by Chen et al. (2008)

E_t is the elastic modulus in tension that, which is assumed to be equal to E_0 in compression; ε_t (=f_t/E_t) is the strain equivalent to the tensile strength of masonry; C_1 = 3; C_2 = 6.93 and ε_v is the strain conforming to zero stress. A small value of ε_v (=0.0003) is used here to imitate the fragile nature of masonry in tension. K_r gives the rate of tension softening of the test specimen. A smooth, slow rate of tension softening is presumed here in order to overcome any numerical difficulties and attain numerical convergence of the analysis.

The stress-strain curves used in the numerical analysis are given as follows:

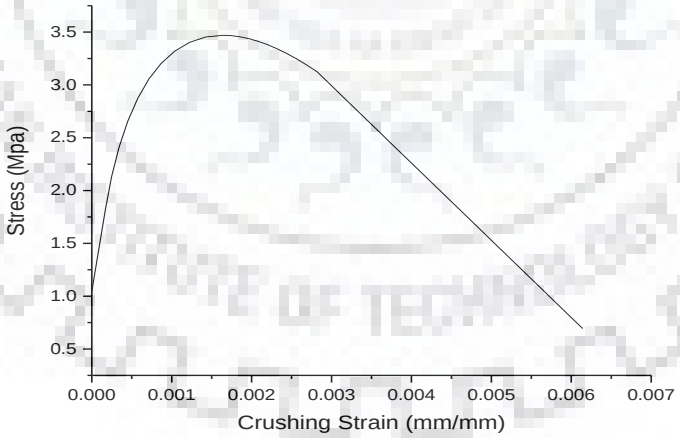

Figure 3.6 Compression behavior in nonlinear range

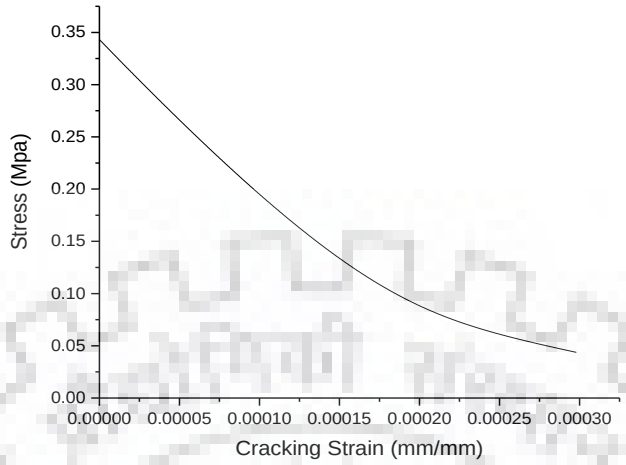

Figure 3.7 Tension behavior in nonlinear range

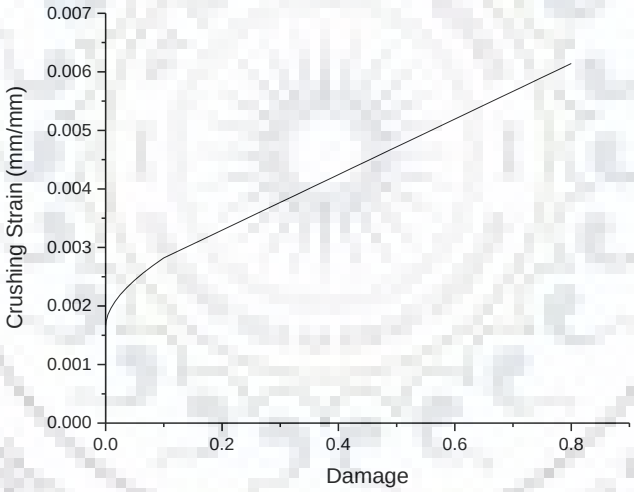

Figure 3.8 Compression damage

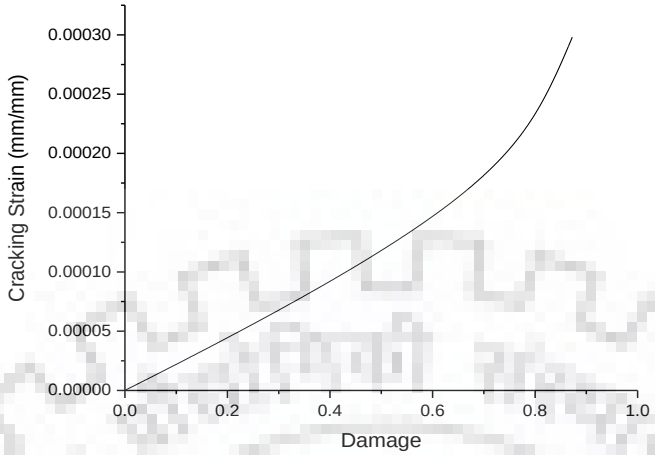

Figure 3.9 Tension damage

3.4.2 Material properties of micro-concrete

Micro-concrete is of M20 grade, having characteristic compressive strength (IS 456 2000) f_{ck} of 20 MPa. Density of concrete was specified (IS 875 Part I 1987) as 2400kg/m3 and Poisson's ratio of 0.2 (Hu et al. 2004) has been utilized in this analysis. The modulus of elasticity of concrete was taken equal to $5000\sqrt{f_{ck}}$ as stated in IS 456 (2000). The strain conforming to the peak stress in concrete has been taken equal to 0.002, and the ultimate strain in unconfined concrete has been taken as 0.005, 0.003 to 0.005 as per to Pillai and Menon (2010).

The model given by Hu et al. (2004) has been used to generate the compression stress strain curve. The numerical formulation is given as follows:

$$\sigma = \frac{E_c \varepsilon_c}{1+(R+R_E-2)\left(\frac{\varepsilon_c}{\varepsilon_0}\right)-(2R-1)\left(\frac{\varepsilon_c}{\varepsilon_0}\right)^2+R\left(\frac{\varepsilon_c}{\varepsilon_0}\right)^3}$$

Where, $R = \frac{R_E(R_\sigma-1)}{(R_\varepsilon-1)} - \frac{1}{R_\varepsilon}$, $R_E = \frac{E_c}{E_0}$, $E_0 = \frac{f_c'}{\varepsilon_0}$ and $R_\sigma = 4, R_\varepsilon = 4, \varepsilon_0 = 0.002$ *and* $\varepsilon_c = 0.005$

The compressive strength of micro-concrete has been considered as 20.14 N/mm^2. Figure 3.10 shows the compression curve generated using the model of Hu et al. (2004) used in the study.

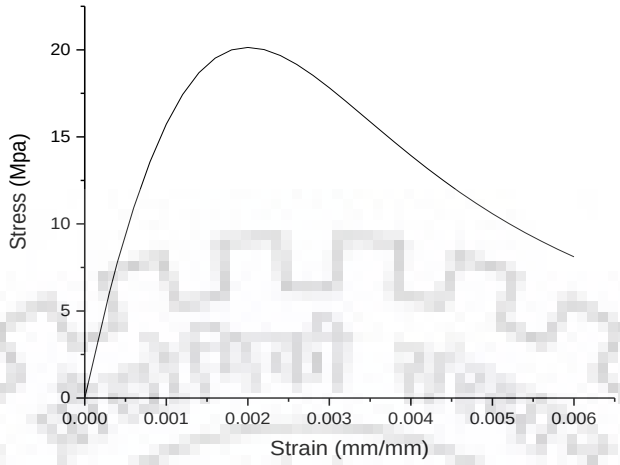

Figure 3.10 Compression curve used in study

To generate the stress-strain curve in tension, the model presented by Vechhio (1990) has been used. This model can be mathematically expressed as follows:

$$f_{c1} = E_c \varepsilon_{c1} \, , 0 \leq \varepsilon_{c1} \leq \varepsilon_{cr}$$

Where, $E_c = \frac{2f_c'}{\varepsilon_0}$ and $\varepsilon_{cr} = \frac{f_{cr}}{E_c}$

After cracking, the behavior of the stress-strain curve is given as follows:

$$f_{c1} = \frac{f_{cr}}{1 + \sqrt{200\varepsilon_{c1}}}$$

The limiting tensile strain of concrete has been stated as 0.0001 (Pillai and Menon 2010). The flexural tensile strength of concrete (f_{cr}) was calculated using the formula 0.7 $\sqrt{f_{ck}}$ based on IS 456 (2000). Figure 3.11 shows the tension curve generated using the model of Vechhio (1990) used in the study.

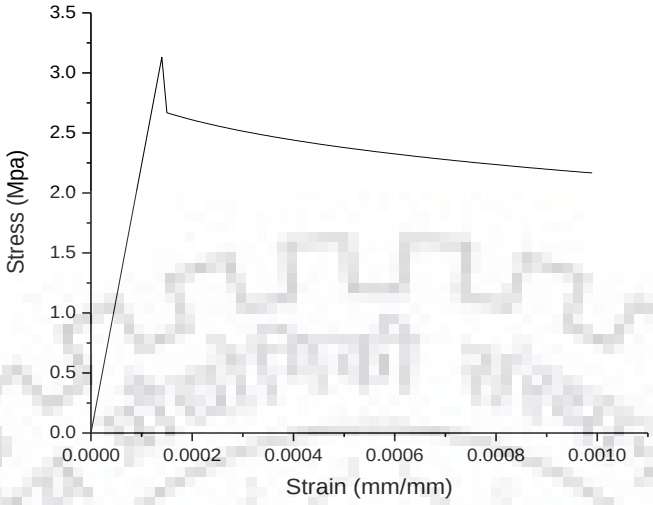

Figure 3.11 Tension curve used in the study

As with masonry, the rudimentary modelling strictures associated to the material properties, have been attained straight from the experimental tests conducted by Kadam (2015). While, the profile of the stress- strain curves, and some supplementary constraints used in the modelling, have been denoted from the pertinent codes and literature.

The curves relating to micro-concrete used in the study are:

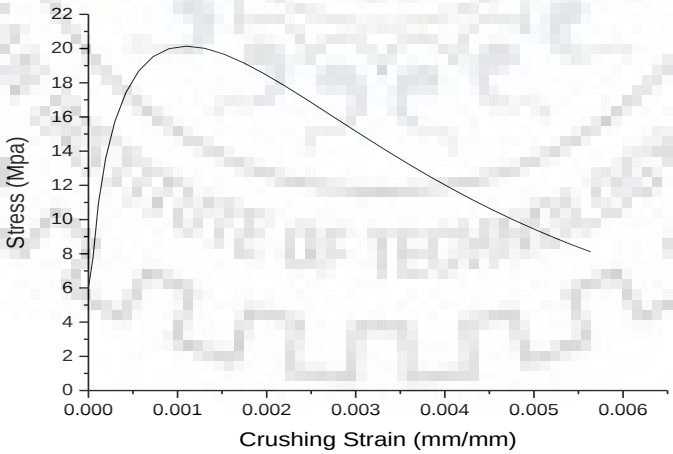

Figure 3.12 Compression behavior in nonlinear range

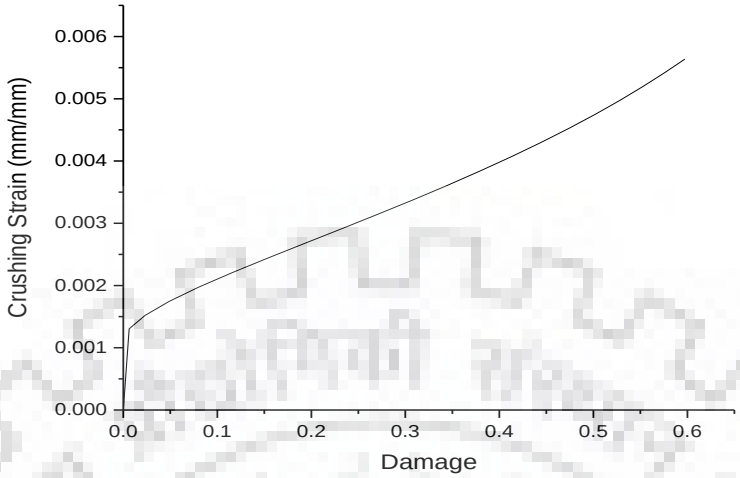

Figure 3.13 Compression damage

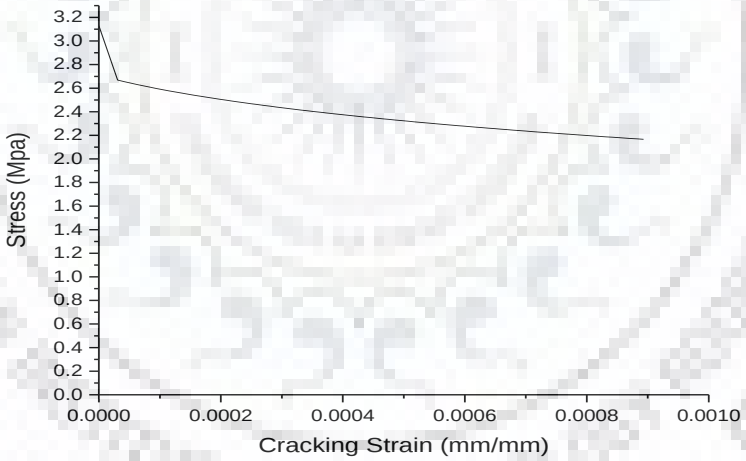

Figure 3.14 Tension behavior in nonlinear range

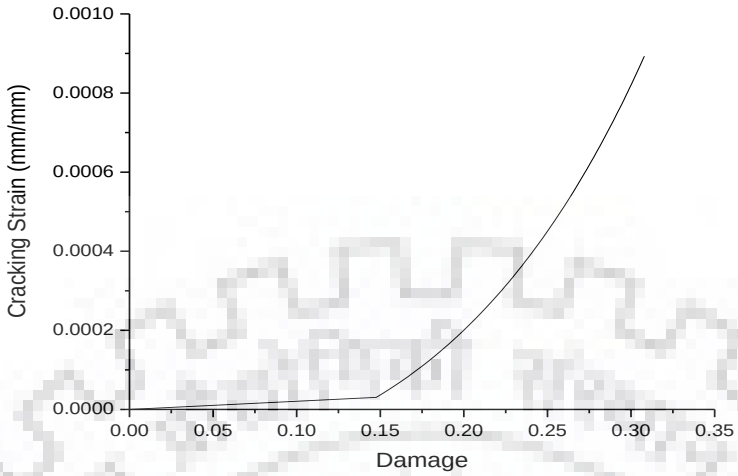

Figure 3.15 Tension damage

The CDP parameters used in modelling for both masonry and micro-concrete are given in tabular form as follows:

Table 3.1 CDP parameters used in modelling masonry and microconcrete

Material	**Elastic modulus(N/mm^2)**	**Poisson's ratio**	**Dilation angle**	**Eccentricity**	f_{bo}/f_{co}	**k**	**Viscosity parameter**
Masonry	2184	0.19	30	0.1	1.16	0.67	0
Concrete	22360	0.19	38	0.1	1.12	0.67	0

The data for the welded wire mesh has been denoted from the tests conducted by Kadam (2015). The stress-strain plot is shown in Figure 3.16. The tensile yield strength of WWM was taken as 850.81 N/mm2 and modulus of elasticity of WWM is taken as 127230 N/mm2. The WWM wire material has very low ductility and fails in an almost brittle manner. The Poisson's ratio of 0.3 and density of 7850 kg/m3 (similar to steel, stated in IS 875 Part I 1987 and Pillai and Menon 2010) has been used for the WWM.

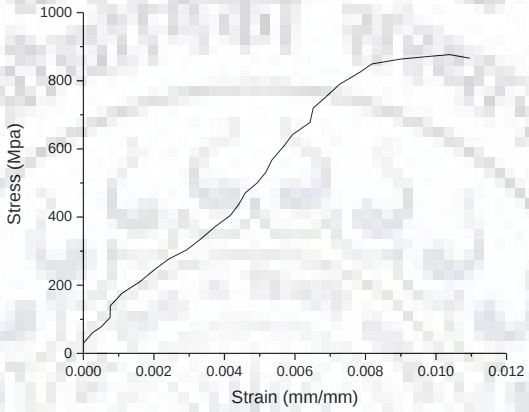

Figure 3.16 Stress-strain curve for WWM

3.5 IN-PLANE TEST

For in-plane testing the diagonal compression test is numerically modelled in ABAQUS. Both a URM specimen and a retrofitted specimen is modelled. The retrofitted specimen consists of a welded wire mesh as reinforcement. The details and results of the analysis are discussed as follows:

3.5.1 URM specimen

For modelling the URM specimen, solid 8-noded linear hexahedral elements (C3D8), frequently recognized as "brick elements" (Oyarzo-Vera et al. 2009) are used. Figure 3.10 describes the elements used in modelling while Figure 3.11 describes the loading and support

conditions used in modelling. As we can see in figure 3.10 and 3.11 below two types of specimens of thickness 110 mm and 230 mm are numerically modelled.

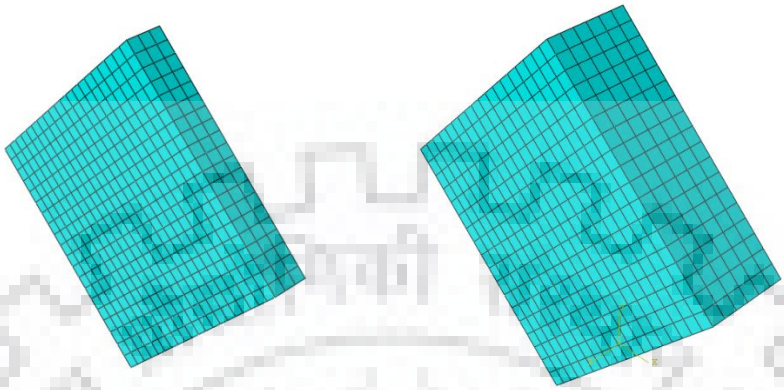

(a) (b)

Figure 3.17 Meshing elements used to model the URM specimen in ABAQUS (a) Single wythe (110 mm thickness) (b) Double wythe (230 mm thickness)

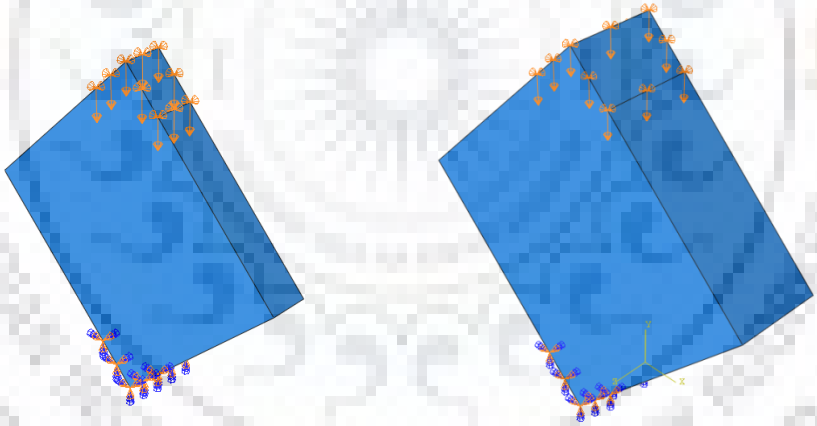

(a) (b)

Figure 3.18 Loading and support conditions modelled in ABAQUS (a) 110 mm thick URM wallette (b) 230 mm thick URM wallette

In the numerical study conducted in ABAQUS it was found that tension damage was the primary mode of failure in the URM specimens in the diagonal compression test. The test results are shown in the form of a stress contour and a damage contour in figures 3.19 to

3.22. No compression damage was observed in the numerical study which was in accordance with the experimental results reported by Kadam (2015).

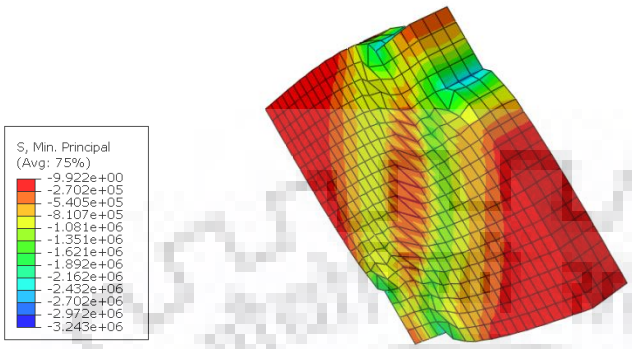

Figure 3.19 Tensile Principal Stress and Deformation of 110 mm thick URM wallette

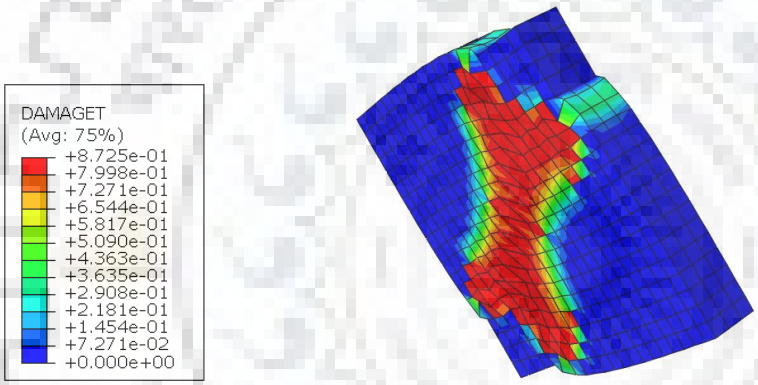

Figure 3.20 Tension damage observed in 110 mm thick URM wallette

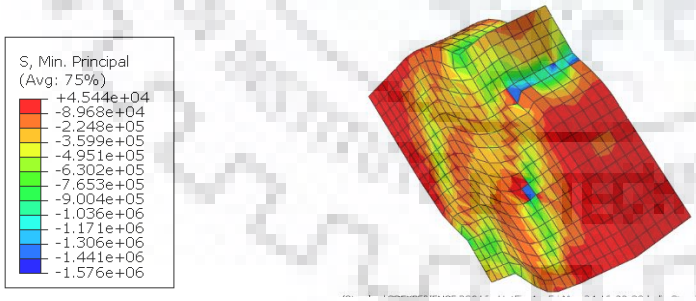

Figure 3.21 Tensile Principal Stress and Deformation of 230 thick mm URM wallete

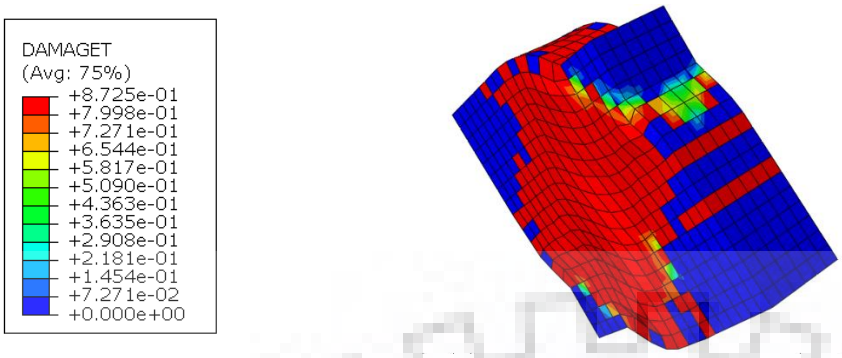

Figure 3.22 Tension damage observed in 230 mm thick URM wallette

In the numerical analysis in ABAQUS different mesh sizes were used in analyzing the URM specimens in diagonal compression test. To analyze the 110 mm thick URM wallette three meshes consisting of 200, 1200 and 2500 elements were analyzed. The results in terms of shear stress-strain curves have been plotted in figure 3.23. It was found that not much difference was observed between 1200 and 2500 elements so consequently the results for 1200 elements were compared with the experimental results as shown in figure 3.24.

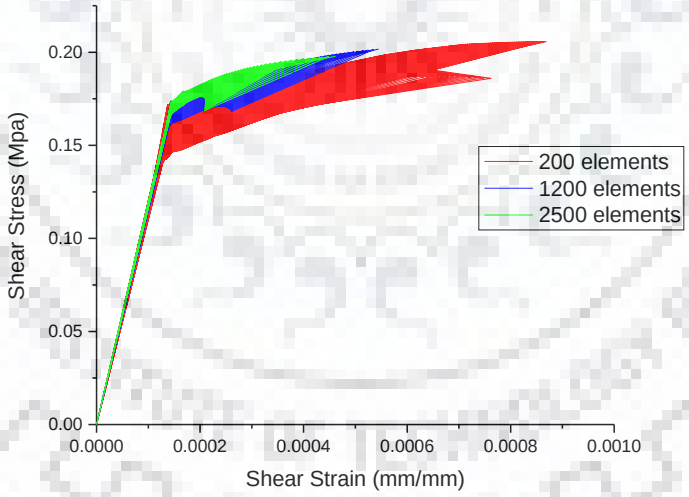

Figure 3.23 Shear stress shear strain curves for different mesh sizes.for 110 mm URM Wallette

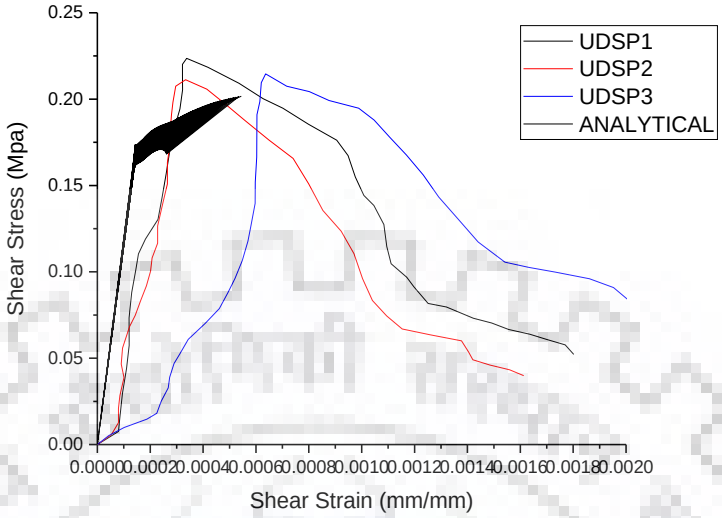

Figure 3.24 Comparison with experimental results for 110 mm thick URM wallette

As we can see from figure 3.24 the peak stress generated in the numerical study did not match the experimental results. This may be due to inaccuracies in the numerical procedure used in analyzing the specimen or due to inadequate mesh size. The peak stress observed from the numerical procedure was 0.2 Mpa but that obtained from the experimental study was 0.2 Mpa

A similar mesh sensitivity analysis was used in the case of the 230 mm thick URM Wallette. Four meshes consisting of 300, 676, 1944 and 2800 elements were used. The results in terms of shear stress-strain curves have been plotted in figure 3.25. It was found that not much difference was observed between 1944 and 2800 elements so consequently the results for 1944 elements were compared with the experimental results as shown in figure 3.26.

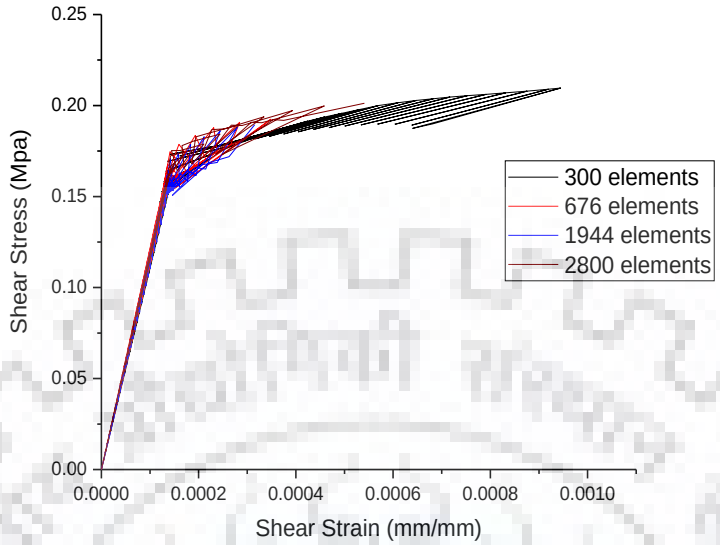

Figure 3.25 Shear stress shear strain curves for different mesh sizes.for 230 mm URM Wallette

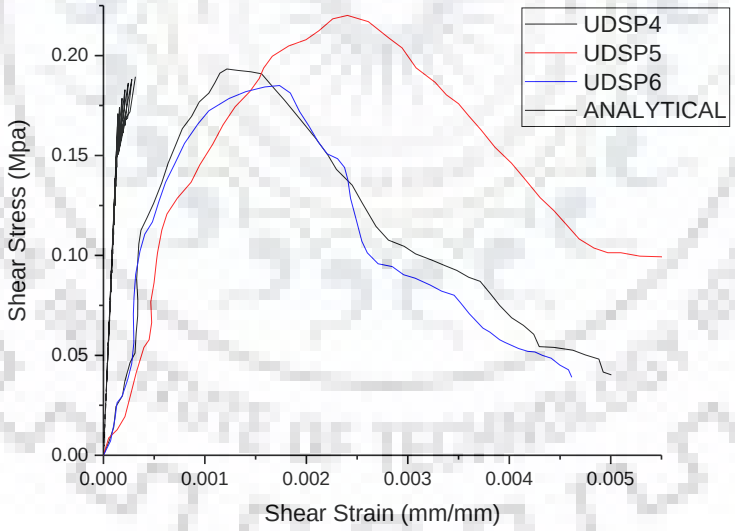

Figure 3.26 Comparison with experimental results for 230 mm thick URM wallette

The numerically obtained peak shear stress of 0.17 Mpa was less than the average shear stress of 0.20 Mpa. Again the reason was inadequate mesh size or inaccuracies in the numerical procedure.

3.5.2 Retrofitted specimen

For modelling the retrofitted specimen, the same, solid 8-noded linear hexahedral elements (C3D8) are used.as shown in figure 3.27 The two micro-concrete layers are also modelled by the same C3D8 elements as shown in figure 3.28 As earlier two specimens of masonry thickness 110 mm and 230 mm are numerically modelled. The welded wire mesh is modelled using truss element as shown in figure 3.29.

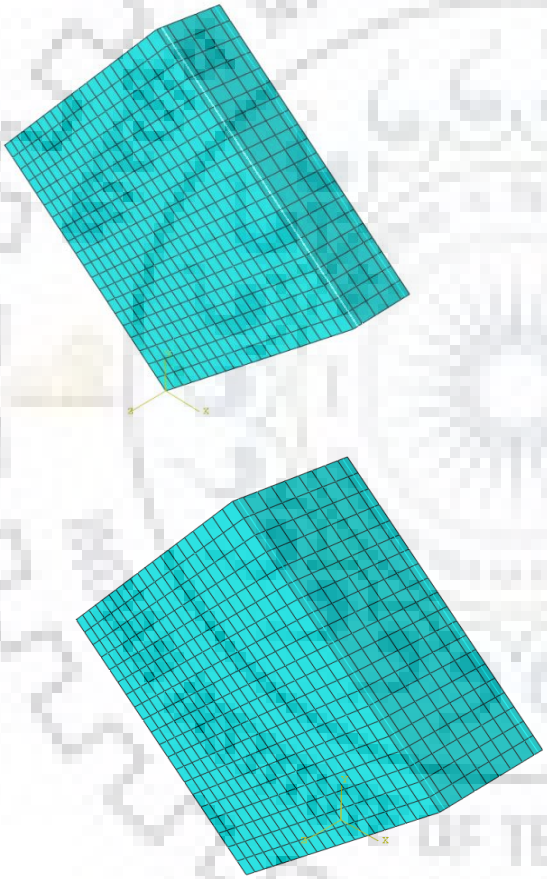

(a) (b)

Figure 3.27 Meshing elements used to model the URM specimen in ABAQUS (a) Single wythe (110 mm thickness) (b) Double wythe (230 mm thickness)

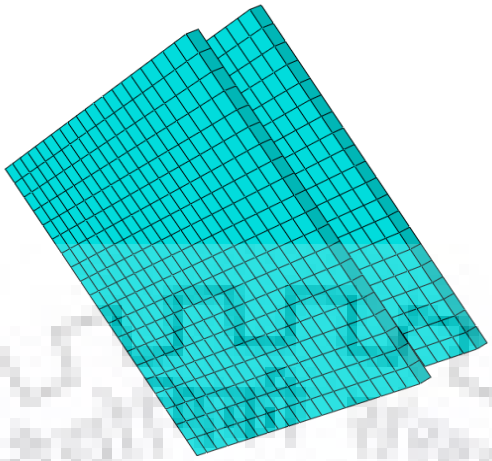

Figure 3.28 Meshing used to model the layer of micro-concrete

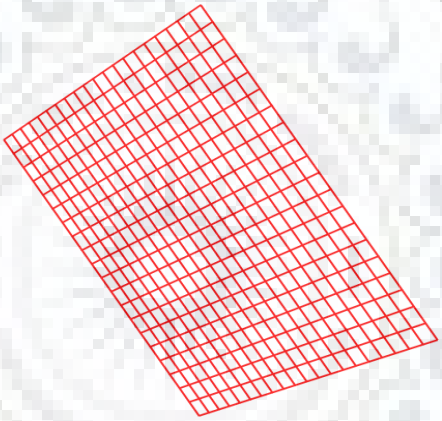

Figure 3.29 Meshing used to model the welded wire mesh

The loading and support conditions and the embedded constraint used to embed the welded wire mesh reinforcement in the numerical model are shown below in figure 3.30 and 3.31.

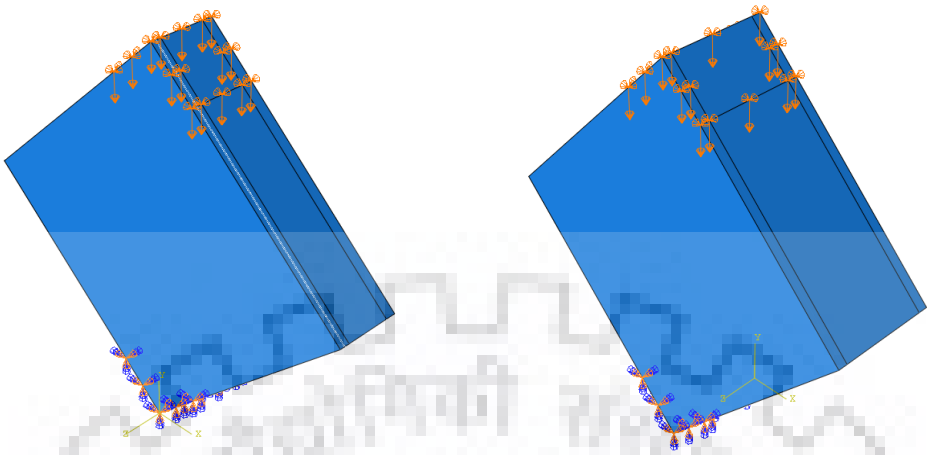

(a) (b)

Figure 3.30 Loading and support conditions modelled in ABAQUS (a) 110 mm thick URM wallette (b) 230 mm thick URM Wallette

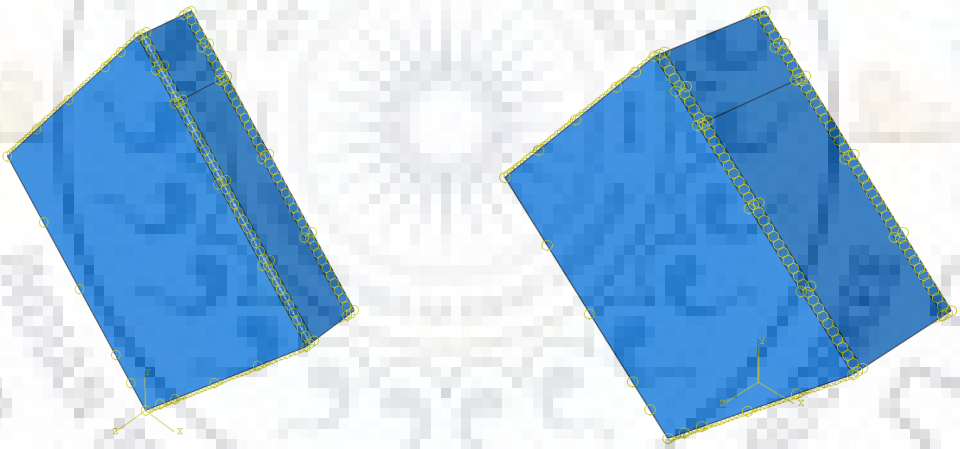

(a) (b)

Figure 3.31 Embedded constraint used to embed the WWM reinforcement in ABAQUS

In the numerical study conducted in ABAQUS it was found that tension damage was the primary mode of failure in the URM specimens in the diagonal compression test. The test results are shown in the form of a stress contour and a damage contour in figures 3.32 to 3.35. No compression damage was observed in the numerical study which was in accordance with the experimental results reported by Kadam (2015).

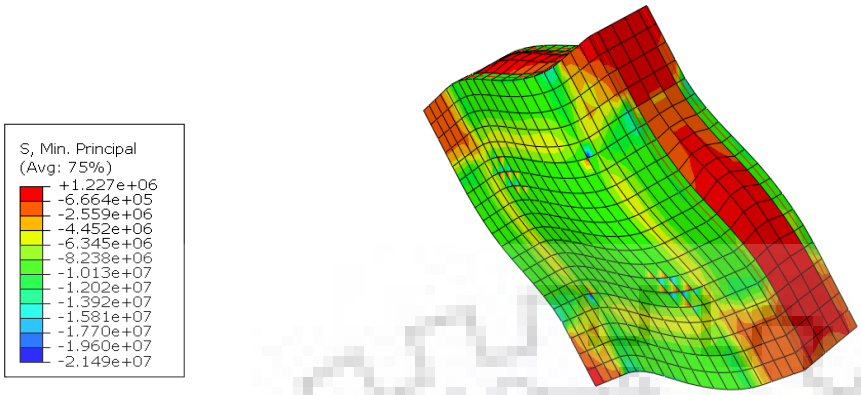

Figure 3.32 Tensile Principal Stress and Deformation of 110 mm thick URM wallette

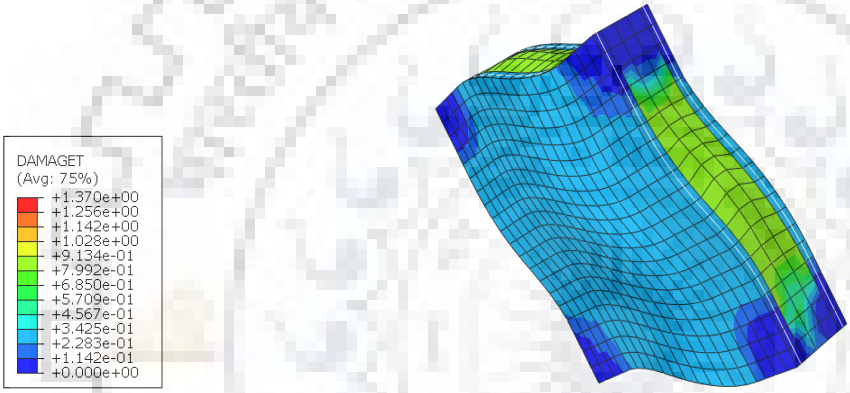

Figure 3.33 Tension damage observed in 110 mm thick URM wallette

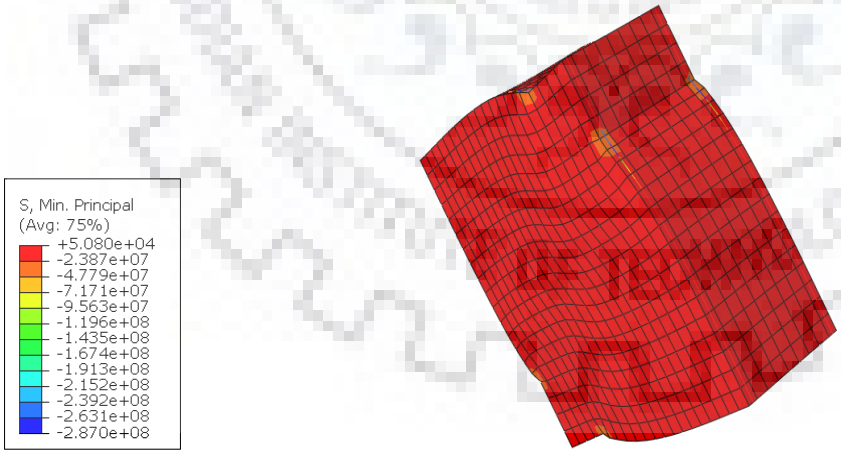

Figure 3.34 Tensile Principal Stress and Deformation of 230 mm thick URM wallette

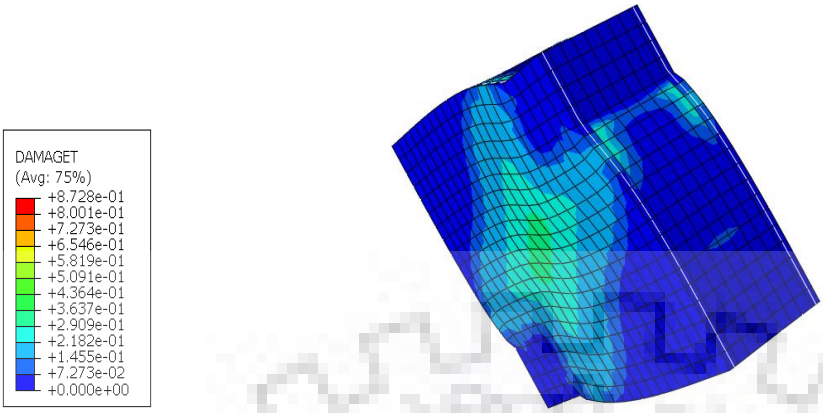

Figure 3.35 Tension damage observed in 230 mm thick URM wallette

To analyze the 110 mm thick URM wallette two meshes consisting of 5360 and 6534 elements were analyzed. The results in terms of shear stress-strain curves have been plotted in figure 3.36. It was found that not much difference was observed between 5360 and 6534 elements so consequently the results for 5360 elements were compared with the experimental results as shown in figure 3.37.

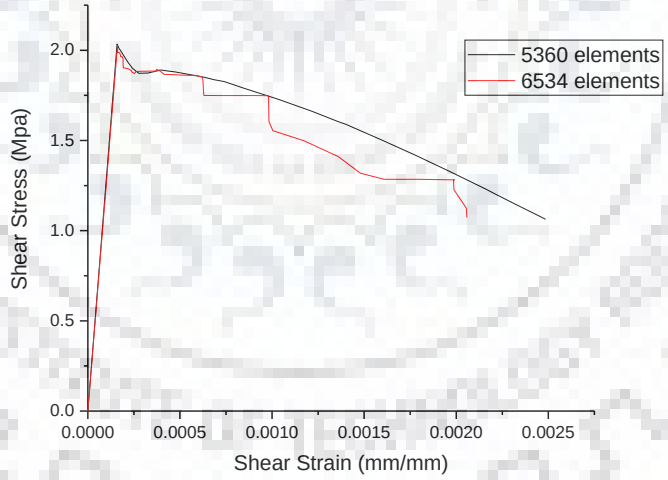

Figure 3.36 Shear stress shear strain curves for different mesh sizes.for 110 mm URM Wallette

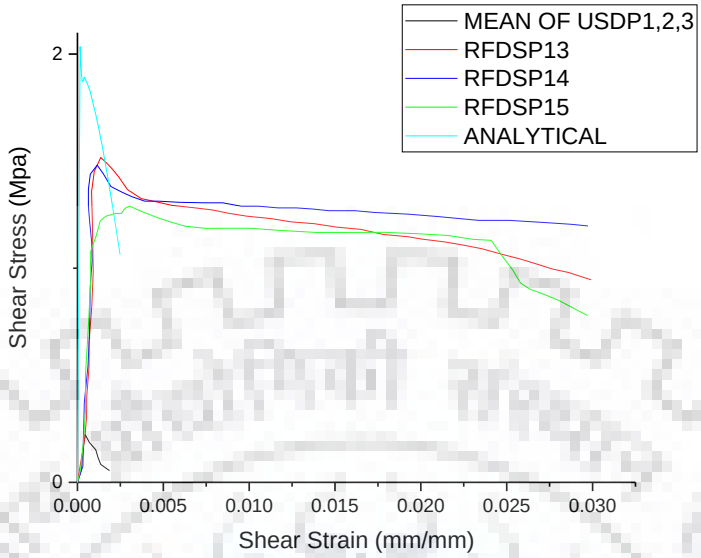

Figure 3.37 Comparison with experimental results for 110 mm thick URM Wallette

The peak shear stress obtained in the numerical study was much higher than the average shear stress obtained in the experimental study conducted by Kadam (2015). The reason for this is the tensile strength parameter which was obtained in the experimental study might have been erroneously reported which led to inaccuracies in the numerical study as the tensile strength parameter greatly influences the results as the damage occurred primarily in tension.

A similar mesh sensitivity analysis was used in the case of the 230 mm thick URM Wallette. Two meshes consisting of 5280 and 6970 elements were used. The results in terms of shear stress-strain curves have been plotted in figure 3.38. It was found that not much difference was observed between 5280 and 6970 elements so consequently the results for 5280 elements were compared with the experimental results as shown in figure 3.39.

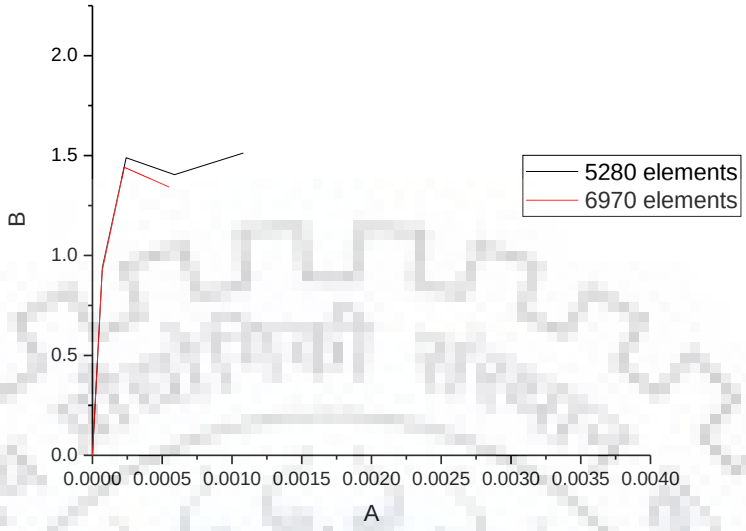

Figure 3.38 Shear stress shear strain curves for different mesh sizes.for 230 mm URM Wallette

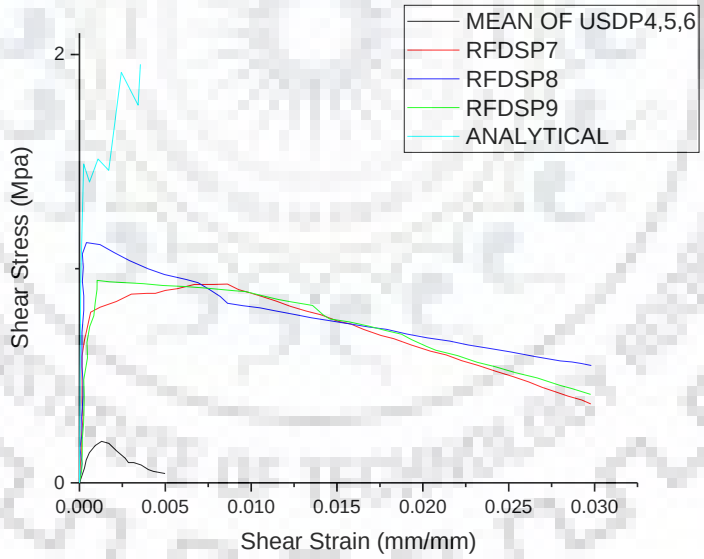

Figure 3.39 Comparison with experimental results for 230 mm thick URM wallette

The peak shear stress obtained in the numerical study was much higher than the average shear stress obtained in the experimental study conducted by Kadam (2015). The reason for this is the tensile strength parameter which was obtained in the experimental study might

have been erroneously reported which led to inaccuracies in the numerical study as the tensile strength parameter greatly influences the results as the damage occurred primarily in tension.

3.6 OUT-OF-PLANE TEST

For out-of-plane testing the four point bending test is numerically modelled in ABAQUS. Both a URM specimen and a retrofitted specimen is modelled. The retrofitted specimen consists of a welded wire mesh as reinforcement. The test is modelled in both perpendicular and parallel to bed joint.The details and results of the analysis are discussed as follows:

3.6.1 URM specimen

For modelling the URM specimen, solid 8-noded linear hexahedral elements (C3D8), frequently recognized as "brick elements" (Oyarzo-Vera et al. 2009) are used. Figure 3.40 describes the elements used in modelling while Figure 3.41 describes the loading and support conditions used in modelling.

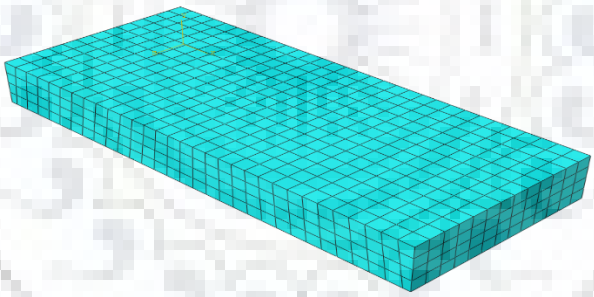

Figure 3.40 Meshing of out-of-plane URM specimen using 8 noded brick element

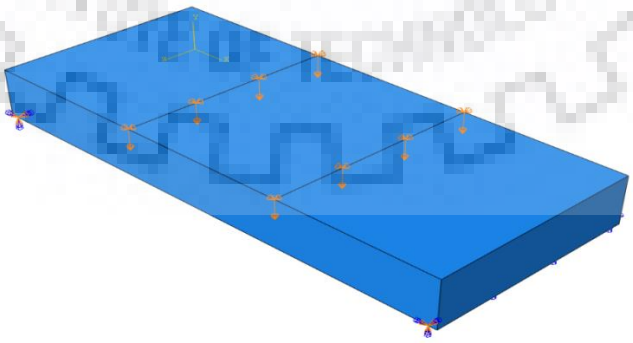

Figure 3.41 Support and loading conditions modelled in ABAQUS

In the numerical study conducted in ABAQUS it was found that tension damage was the primary mode of failure in the URM specimens in the diagonal compression test. The test results are shown in the form of a stress contour and a damage contour in figures 3.42 to 3.45. No compression damage was observed in the numerical study which was in accordance with the experimental results reported by Kadam (2015).

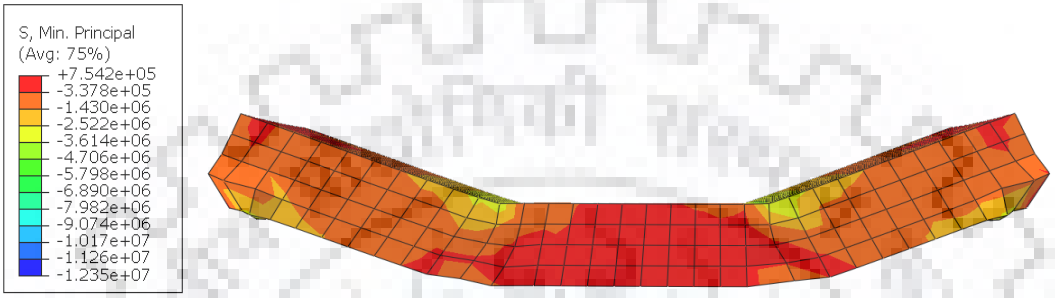

Figure 3.42 Tensile Principal Stress and Deformation parallel to bed joint

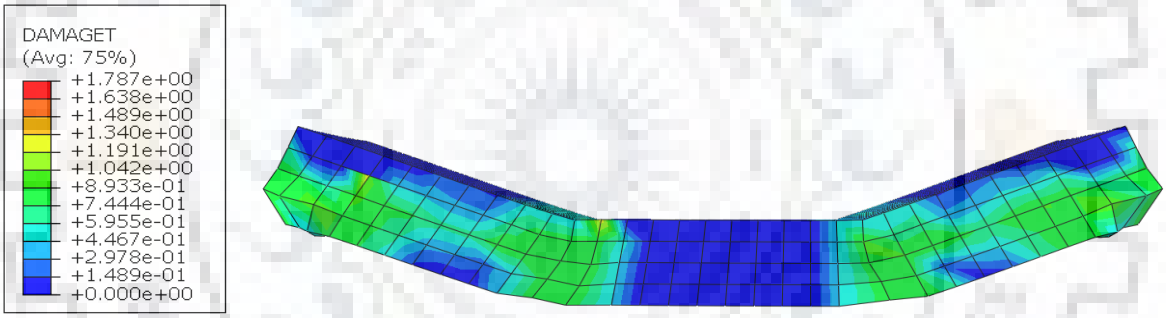

Figure 3.43 Tension damage observed parallel to bed joint

Figure 3.44 Tensile Principal Stress and Deformation perpendicular to bed joint

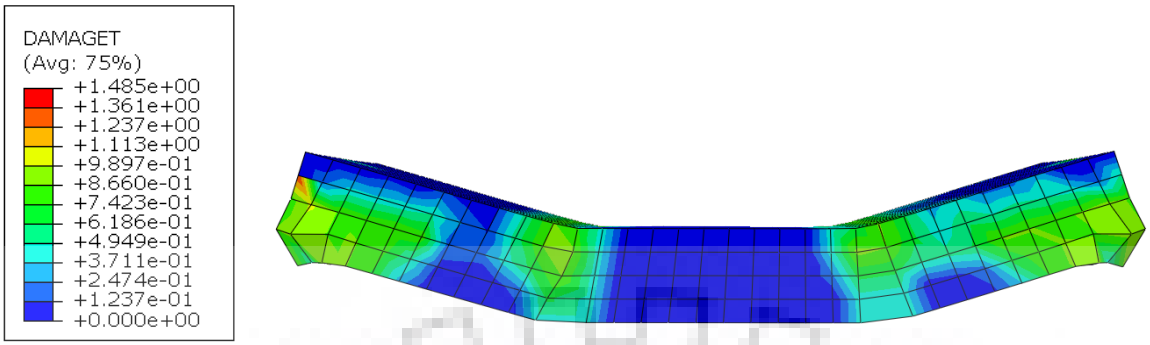

Figure 3.45 Tension damage observed perpendicular to bed joint

To analyze the URM wallette parallel to bed joint, two meshes consisting of 378 and 1612 elements were analyzed. The results in terms of shear stress-strain curves have been plotted in figure 3.46. The results for 1612 elements were compared with the experimental results as shown in figure 3.47.

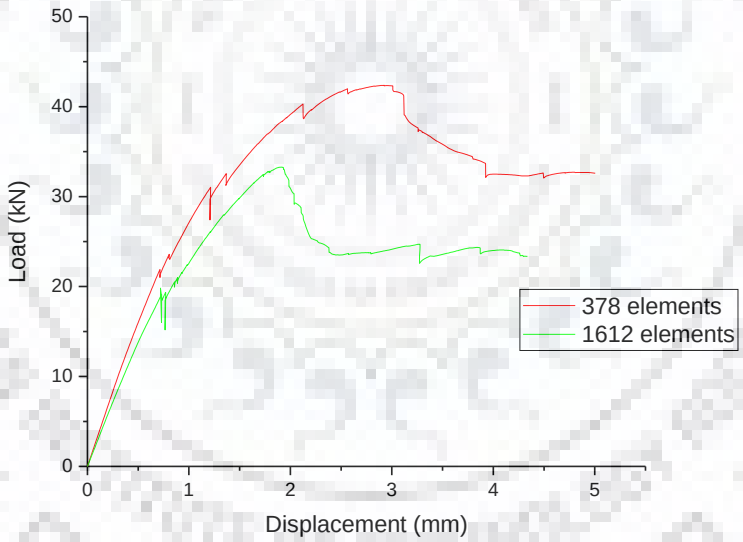

Figure 3.46 Load-displacement curve parallel to bed joint

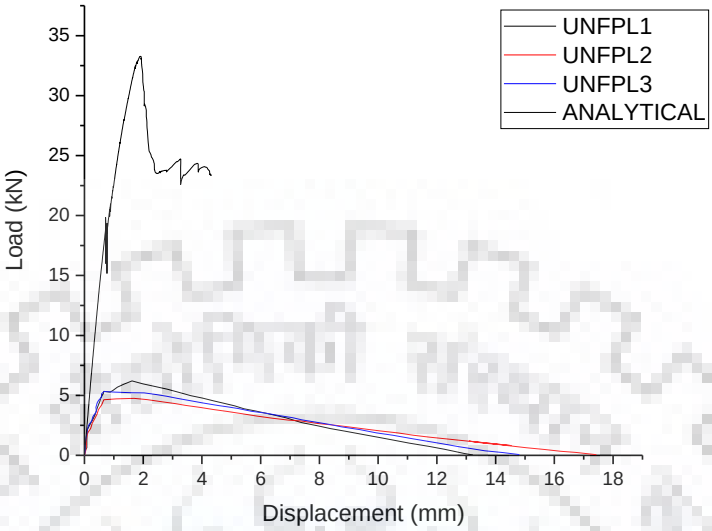

Figure 3.47 Comparison with experimental results parallel to bed joint

The peak load in the load-displacement did not match the value average value obtained from the experimental tests. The reason for this is the tensile strength parameter which was obtained in the experimental study might have been erroneously reported which led to inaccuracies in the numerical study as the tensile strength parameter greatly influences the results as the damage occurred primarily in tension.

3.6.2 Retrofitted specimen

For modelling the retrofitted specimen, the same, solid 8-noded linear hexahedral elements (C3D8) are used.as shown in figure 3.48. As earlier two specimens of masonry both perpendicular to bed joint and parallel to bed joint were modelled. The welded wire mesh is modelled using truss element as shown in figure 3.49.

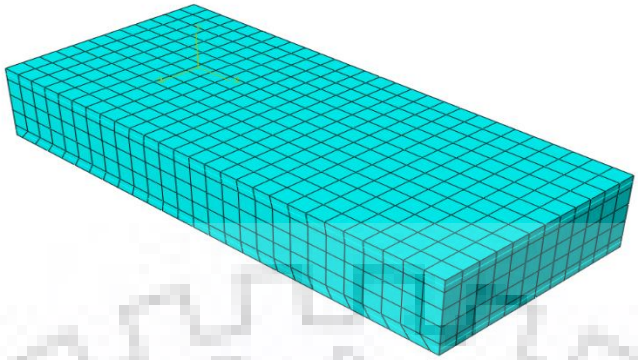

Figure 3.48 Meshing of out-of-plane URM specimen using 8 noded brick element

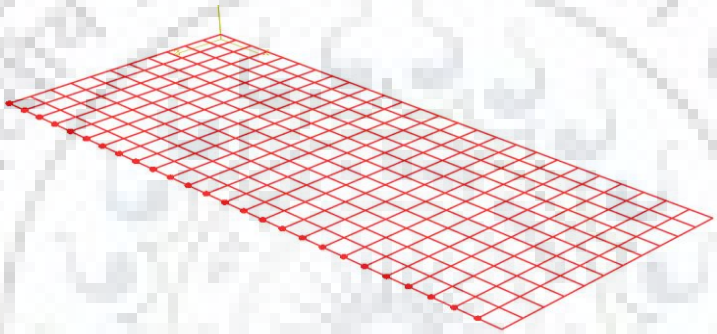

Figure 3.49 Meshing used to model the welded wire mesh

The loading and support conditions have been modelled as follows:

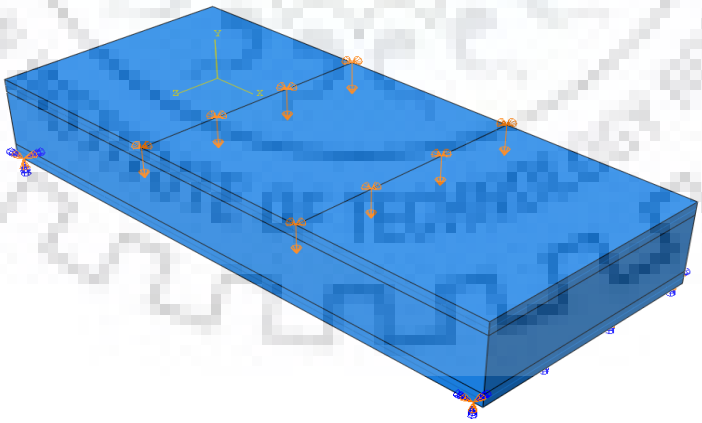

Figure 3.50 Loading and support conditions modelled in ABAQUS

The embedded constraint used to embed the welded wire mesh reinforcement in the numerical model is shown below in figure 3.51.

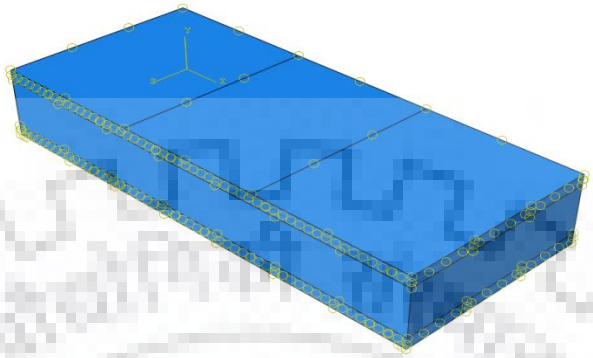

Figure 3.51 Embedded constraint used to embed the WWM reinforcement in ABAQUS

In the numerical study conducted in ABAQUS it was found that tension damage was the primary mode of failure in the URM specimens in the diagonal compression test. The test results are shown in the form of a stress contour and a damage contour in figures 3.51 to 3.54. No compression damage was observed in the numerical study which was in accordance with the experimental results reported by Kadam (2015).

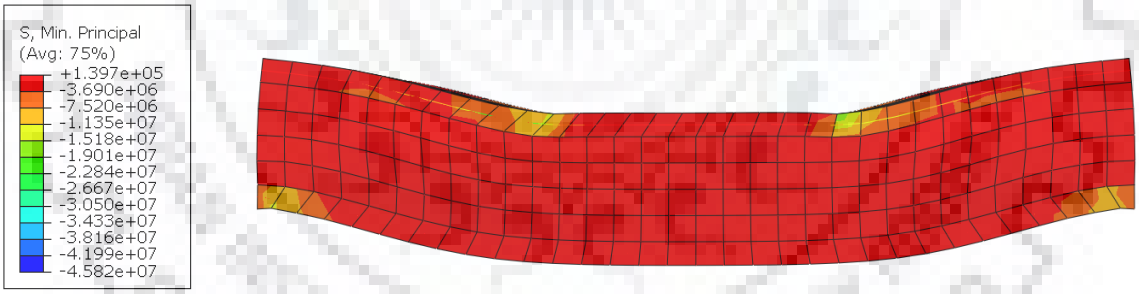

Figure 3.52 Tensile Principal Stress and Deformation parallel to bed joint

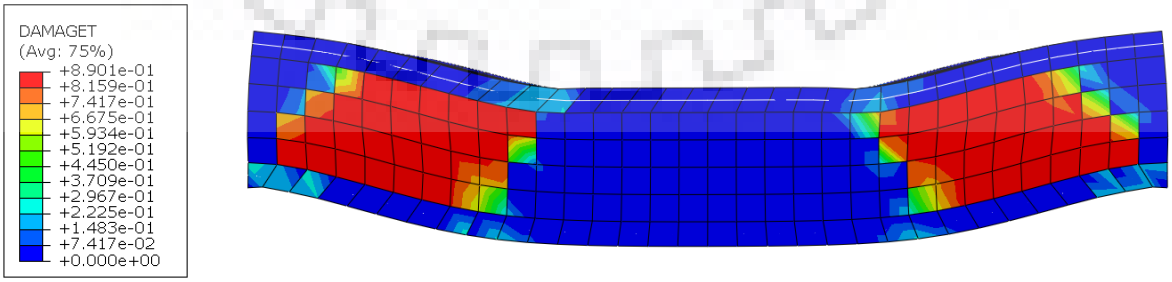

Figure 3.53 Tension damage observed parallel to bed joint

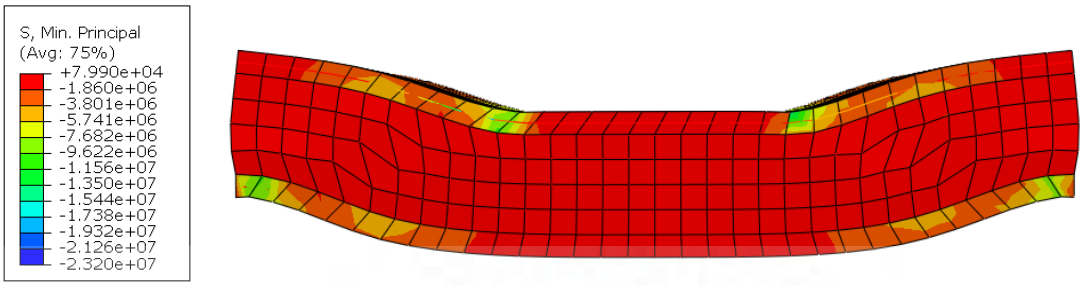

Figure 3.54 Tensile Principal Stress and Deformation perpendicular to bed joint

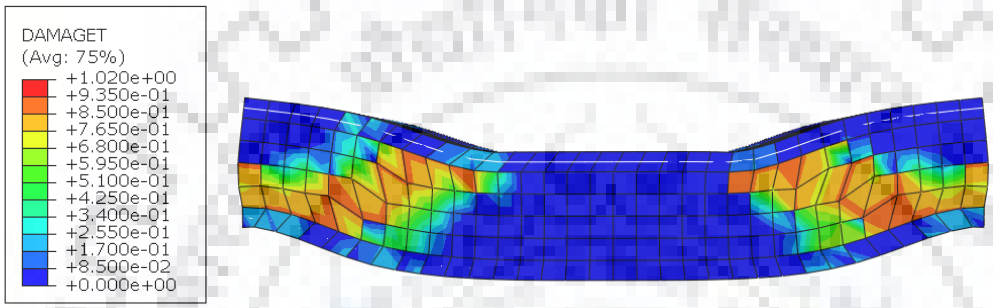

Figure 3.55 Tension damage observed perpendicular to bed joint

To analyze the URM wallette parallel to bed joint, two meshes consisting of 2890 and 3958 elements were analyzed. The results in terms of shear stress-strain curves have been plotted in figure 3.56. The results for 3958 elements were compared with the experimental results as shown in figure 3.57.

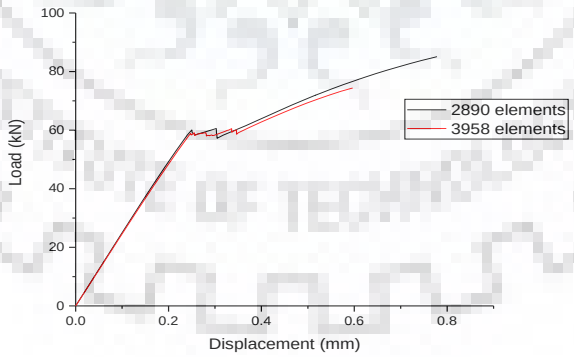

Figure 3.56 Load-displacement curve parallel to bed joint

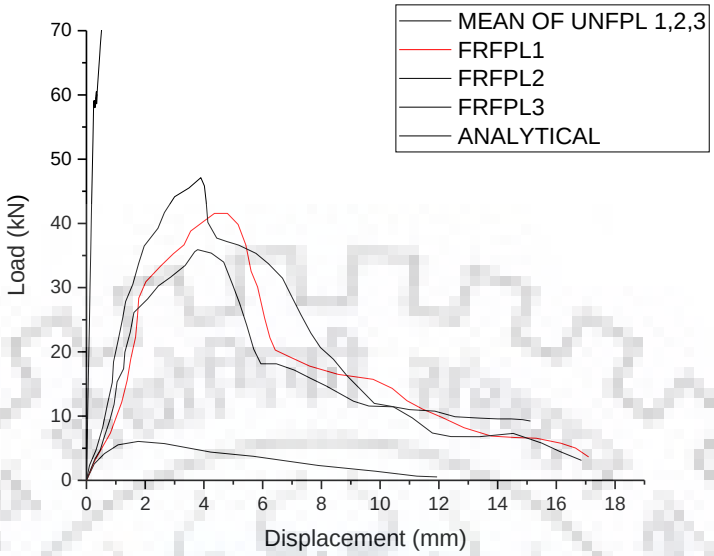

Figure 3.57 Comparison with experimental results parallel to bed joint

The peak load in the load-displacement did not match the value average value obtained from the experimental tests. The reason for this is the tensile strength parameter which was obtained in the experimental study might have been erroneously reported which led to inaccuracies in the numerical study as the tensile strength parameter greatly influences the results as the damage occurred primarily in tension.

A similar mesh sensitivity analysis was used in the case of perpendicular to bed joint. Two meshes consisting of 2890 and 3958 elements were used. The results in terms of load-displacement curves have been plotted in figure 3.58. The results for 3958 elements were compared with the experimental results as shown in figure 3.59.

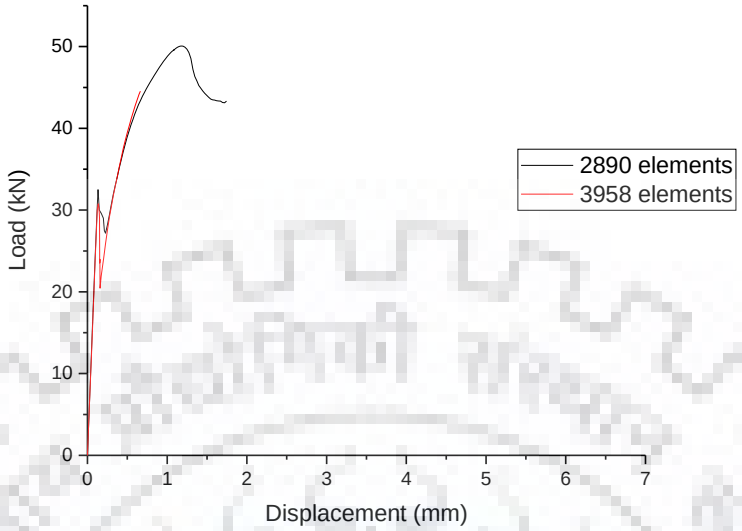

Figure 3.58 Load-displacement curve perpendicular to bed joint

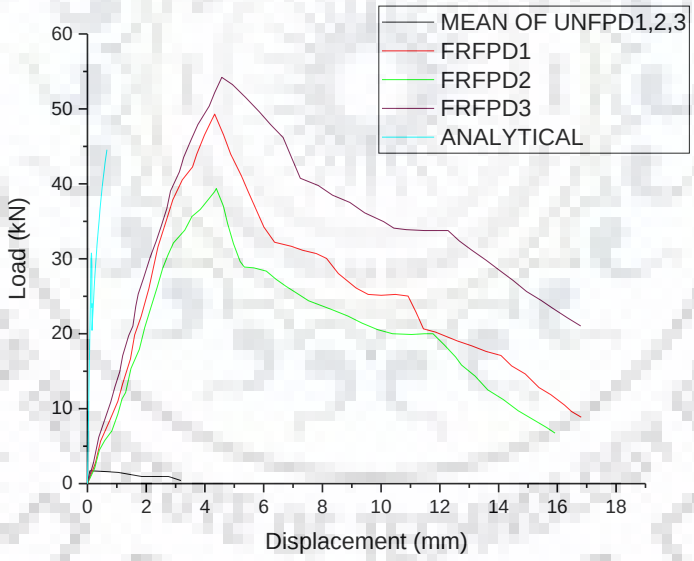

Figure 3.59 Comparison with experimental results perpendicular to bed joint

The peak load in the load-displacement did not match the value average value obtained from the experimental tests. The reason for this is the tensile strength parameter which was obtained in the experimental study might have been erroneously reported which led to

inaccuracies in the numerical study as the tensile strength parameter greatly influences the results as the damage occurred primarily in tension.

Chapter 4

Equivalent Frame Modelling

4.1 IN-PLANE MODELLING

A substantial quantity of previous investigational investigation has been devoted to understanding the performance of unreinforced masonry (URM) walls when exposed to in-plane and out-of-plane loading [Tomazevic et al. (1996); Magenes and Calvi, (1997)]. It has been witnessed that the lateral strength, stiffness degradation, and prime mode of failure in the walls rest on on the collective outcome of axial and lateral loads, boundary constraints, aspect ratio (height/width ratio), and material features. As per ASCE 41-17, URM has five key modes of failure. Deformation controlled in-plane actions of URM walls comprise rocking and bed-joint sliding that contains stair-step cracking through head and bed joints. Force-controlled in-plane actions of URM walls comprise toe crushing, diagonal tension that causes cracking through the masonry units, and vertical compression.

4.1.1 Rocking failure

The strength in in-plane rocking shall be calculated as per the following equation

$$Q_{CE} = V_r = 0.9(\alpha P_D + 0.5P_w)L/h_{eff}$$

Where,

h_{eff} = Height to resultant of seismic force

L = Length of wall or wall pier

P_D = Superimposed dead load on top of wall or wall pier being considered

P_w = Self weight of wall or pier

V_r = Strength of wall or wall pier based on rocking

α = Factor equal to 0.5 for fixed-free cantilever wall, or equal to 1.0 for fixed-fixed wall pier.

4.1.2 Bed-joint sliding failure

The expected initial bed-joint sliding strength is given as:

$$Q_{CE} = V_{bjs1} = v_{me} A_n$$

Where,

A_n = Area of net mortared or grouted section of a wall or wall pier;

v_{me} = Expected bed-joint sliding shear strength

V_{bjs1} = Expected initial shear strength of wall or pier based on bed-joint sliding shear strength.

Expected final bed-joint sliding strength is given as:

$$Q_{CE,F} = V_{bjs2} = 0.5 P_D$$

Where,

P_D = Superimposed dead load on wall or wall pier

V_{bjs2} = Expected final shear strength of wall or pier based on bed-joint sliding shear strength.

4.1.3 Toe-crushing failure

Lower bound toe crushing strength is given as:

$$Q_{CL} = V_{tc} = (\alpha P_D + 0.5 P_w)\left(\frac{L}{h_{eff}}\right)\left(1 - \frac{f_a}{0.7 f'_m}\right)$$

Where,

f_a = Axial compression stress caused by gravity loads

f'_m = Lower-bound masonry compressive strength

P_D = Superimposed dead load at the top of the wall or wall pier under consideration;

P_w = Self-weight of the wall pier

V_{tc} = Lower-bound shear strength based on toe crushing for a wall or wall pier.

4.1.4 Diagonal tension failure

Lower bound diagonal tensile strength is given as:

$$Q_{CL} = V_{dt} = f'_{dt} A_n \beta \sqrt{1 + \frac{f_a}{f'_{dt}}}$$

Where,

A_n = Area of net mortared and/or grouted section of a wall or wall pier

β = 0.67 for L/heff < 0.67, L/heff when 0.67 ≥ L/heff ≤ 1.0, and 1.0 when L/heff > 1.0

h_{eff} = Height to resultant of seismic force

L = Length of wall or wall pier

f_a = Axial compression stress caused by gravity loads

f'_{dt} = Lower-bound masonry diagonal tension strength; and

V_{dt} = Lower-bound shear strength based on diagonal tension stress for wall or pier.

4.1.5 Vertical compression failure

$$Q_{CL} = P_{CL} = 0.80(0.85 f'_m A_n)$$

Where,

f'_m = Lower-bound compressive strength

A_n = Area of net mortared and/or grouted section.

4.2 EQUIVALENT FRAME ELEMENT

In Equivalent Frame Modeling, the piers and spandrels are modelled as nonlinear inelastic skeletal (frame) elements having shear and flexural distortions. The contacts amongst piers and spandrels are habitually well-thought-out as unyielding. The piers are modelled by bearing in mind their effective height. Dolce (1989) projected the notion of effective height

and has provided terminologies to compute effective height of the piers in masonry buildings. Figure 4.1 shows the graphic perception of equivalent frame romanticism of a masonry wall and of effective height of discrete masonry piers as suggested by Dolce.

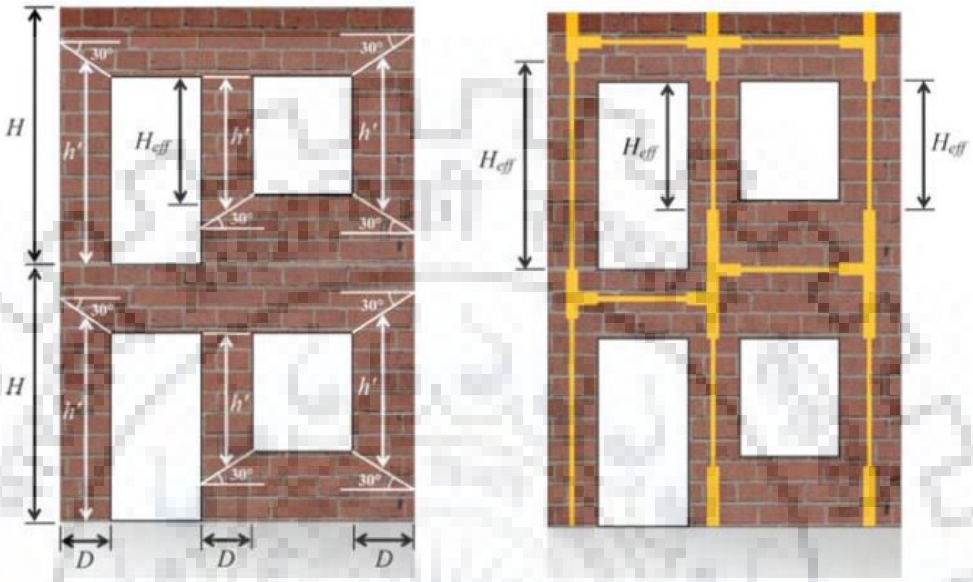

Figure 4.1 2D Illustration of a Representative Masonry Wall Presenting: (a) Effective Height of Piers, as per Dolce (1989); and (b) Equivalent Frame Model

Dolce's standard for calculation of effective height of piers, shown in Figure 4.1, can be articulated numerically as:

$$H_{eff} = h' + \frac{1}{3h'} D(H - h')$$

Where, h', D and H_{eff} are shown in figure 4.1. In the present study, flexure, diagonal shear and sliding shear have been well thought-out as possible failure modes for piers; while simply shear failure has been well-thought-out as probable failure mode for spandrels. The flexural, diagonal shear and sliding shear capacity of the individual piers have been evaluated by the equations given by Pasticier et al.

The flexural capacity is given as:

$$M_u = \frac{\sigma_0 D^2 t}{2}\left(1 - \frac{\sigma_0}{K' f_d}\right)$$

The diagonal shear capacity is given as:

$$V^u = \frac{1.5 f_{vod} Dt}{\xi} \sqrt{1 + \frac{\sigma_0}{1.5 f_{vod}}}$$

The sliding shear capacity is given as:

$$V_s^u = \frac{1.5 f_{vod} + \frac{\mu_f \sigma_0}{\gamma_m}}{1 + \frac{3H_0}{D\sigma_0} f_{vod}}$$

4.3 BACK-BONE CURVE

The backbone curve is given in ASCE 41(2017) as shown in figure 4.2

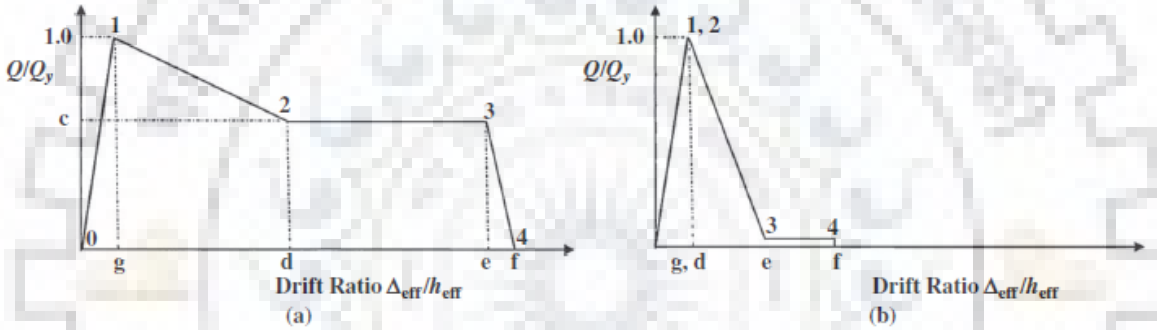

Figure 4.2 Typical Generalized Force. (a) Deformation Relationship for Deformation-Controlled Actions for Reinforced or Unreinforced Masonry; and (b) Deformation Relation for Force Controlled Actions for Reinforced or Unreinforced Masonry

The values of c,d,e,f and g are given in ASCE 41(2017) as shown in the table below:

Table 4.1 Force-deformation relations for in-plane URM walls as per ASCE 41(2017)

Limiting behavior mode	**Residual strength ratio**	**d (%)**	**e (%)**	**f (%)**
Wall and Wall Pier Rocking	$V_{tc.r}/V_r$	$100\Delta_{tc,r}/h_{eff}$	$100\Delta_{tc,r}/h_{eff}$	$100(\Delta_{tc,r} + \Delta_y)/h_{eff}$
Wall and	V_{bjs2}/V_{bjs1}	0.4	1.0	$1.0 + 100\Delta_y)/h$

Wall Pier Bed-Joint Sliding				
Spandrels with prismatic lintels	$Min(V_{fl,r}, V_{s,r})/Min(V_{fl},$	0.3	3.0	3.1
Spandrels with Shallow Arch Lintels	$Min(V_{fl,r}, V_{s,r})/Min(V_{fl},$	0.3	0.75	0.85

4.4 ACCEPTANE CRITERIA

4.4.1 In-plane action

In-plane lateral shear of unreinforced masonry walls and wall piers in each line of resistance is well thought-out as a deformation-controlled action if the anticipated lateral rocking strength or bed joint sliding strength of each wall or wall pier in the line of resistance is less than the lower-bound lateral strength of each wall or wall pier limited by diagonal tension or toe crushing.URM walls that do not comply with the standards for deformation-controlled components shall be well thought-out as force-controlled constituents. Axial compression on URM wall components shall be well-thought-out as a force-controlled action.

4.4.2 Out-of-plane action

For the Immediate Occupancy Structural Performance Level, flexural cracking in URM walls caused by out-of-plane inertial loading is not to be allowed as per ASCE 41(2017). Bed-joint flexural tensile strength is limited by Table 11-2a of ASCE 41(2017). If $v_{tL} \leq 30$ lb/in.2 (206.8 kPa), flexural cracking in URM walls instigated by out-of-plane inertial loading shall be allowed for the Life Safety and Collapse Prevention Structural Performance Levels, providing that cracked wall segments remain steady during dynamic excitation. For the

Collapse Prevention Structural Performance Level, walls spanning vertically shall have a height-to-thickness (h⁄t) ratio less than or equal to that given in Table 11-5 of ASCE 41(2017) Life Safety Acceptance Criteria for URM Walls Subject to Out-of-Plane Actions. Eqs. (11-27a) through (11-27d) shall be utilized to evaluate the Life Safety Structural Performance Level. A wall shall be well-thought-out as linked to stiff diaphragms if the stretchiest diaphragm coupled to the wall has a period TDIAPH ≤ 0.2 s. A wall at a given story shall be well-thought-out as linked to flexible diaphragms if the most flexible diaphragm connected to the wall has a period TDIAPH ≥ 0.5 s. Linear interpolation of SaDIAPH, Ca, Cpl, and Cg in Eq. founded on the diaphragm period shall be allowed for 0.5 s > TDIAPH > 0.2 s. Periods of the diaphragms shall be based on diaphragm stiffnesses. Half of the wall height (or any parapet for top-level walls) above and below the diaphragm in question shall be considered in evaluation of tributary mass for the diaphragm period.

The acceptance criteria for performance level is given as follows:

Table 4.2 Acceptance criteria for performance level

IO	**LS**	**CP**
0.1	$0.4h_{eff}/L$ but not greater than 1.50%	$0.6h_{eff}/L$ but not greater than 2.25%
0.1	$0.6h_{eff}/L$ but not greater than 2.25%	$100\Delta_{tc,r}/h_{eff}$ but not greater than 2.5%
0.1	0.75	1.0
0.1	2.25	3.0
0.1	0.56	0.75

Chapter 5

Numerical Study

5.1 EXAMPLE BUILDING

The example building modelled in the study is a half scale masonry model which was experimentally analyzed by Kadam (2015). The schematics of the building are given as follows:

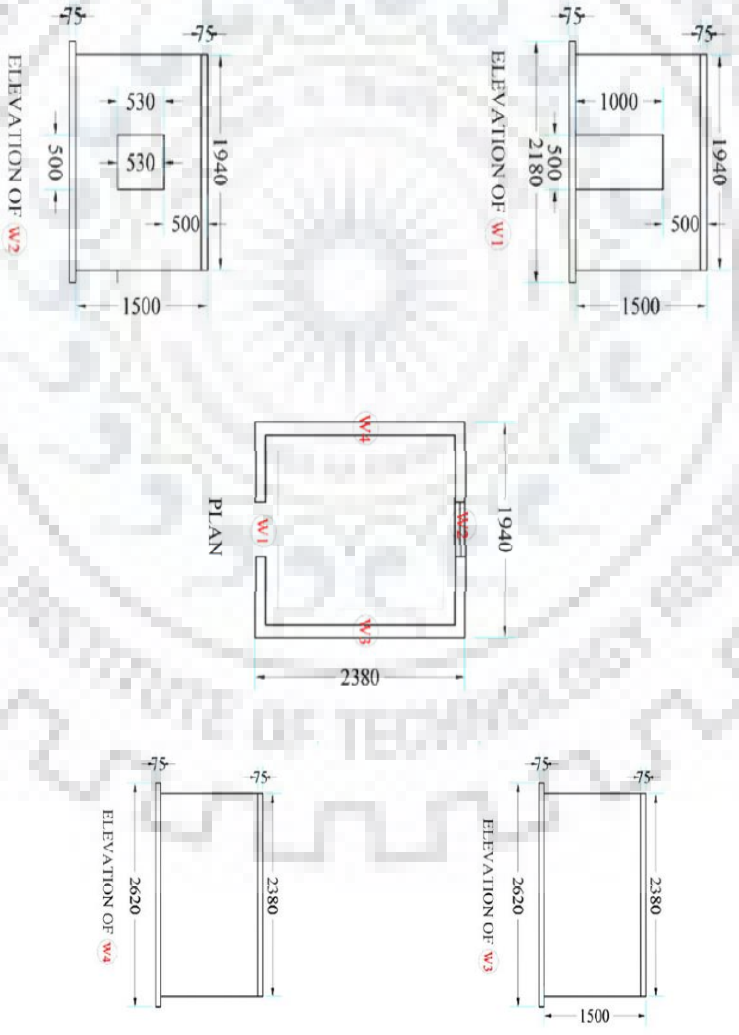

Figure 5.1 Plan and elevation of half scale masonry model

The masonry half scale model was prepared by a skilled mason using half scale burnt clay bricks of sizes 118×58×37 mm and 8-10 mm thick mortar joints using 1:6 cement sand mortar. Two gaps were provided in the model in the form of a window and a door, in the walls along the loading direction and roof comprised of regular RC slab (Kadam 2015).

5.2 FE MODELLING AND ANALYSIS

For FE modelling of the masonry half scale model, CDP model is used to model both the nonlinearity of masonry and the nonlinearity of the RC roof slab. Solid 8-noded linear hexahedral elements (C3D8) are used again to model the building in ABAQUS. The details of the elements used to model the structure are shown in figure 5.2.

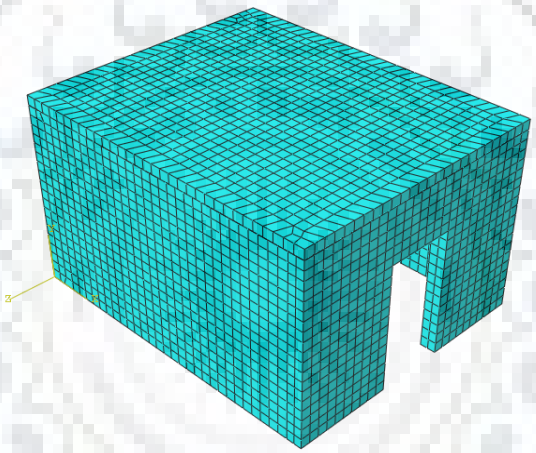

Figure 5.2 Meshing of half scale masonry building using 8 noded brick element

5.2.1 Modal analysis

The modal analysis is performed in ABAQUS using the frequency analysis module available in ABAQUS. The meshing is as shown in figure 5.2. The support conditions are shown in figure 5.3.

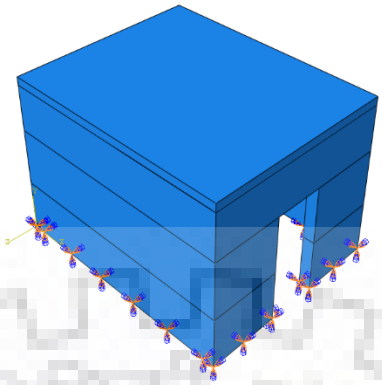

Figure 5.3 Support conditions for modal analysis

The modal analysis was performed for 12 modes but the first mode was found to be dominant. The frequency of the first mode is reported as …. The first mode is shown in figure 5.4.

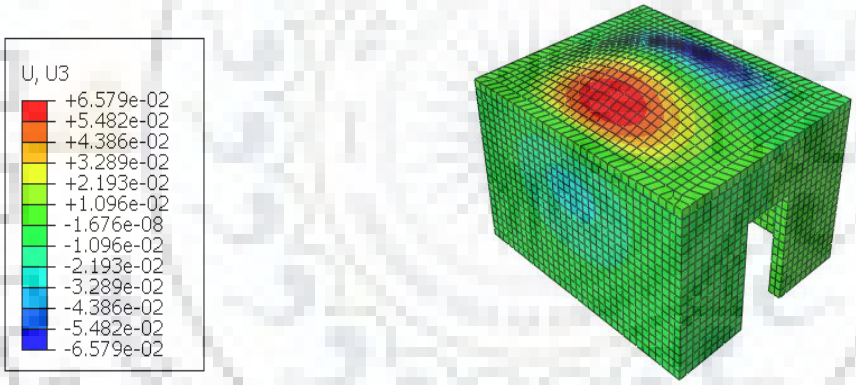

Figure 5.4 First mode shape of masonry half scale model analyzed in ABAQUS

5.2.2 Nonlinear Static (Pushover) analysis

The meshing used for the pushover analysis is the same as shown in figure 5.2. The displacement controlled load was provided at the roof level of the half scale model while the base was kept fixed. The support and loading conditions are shown in figure 5.5.

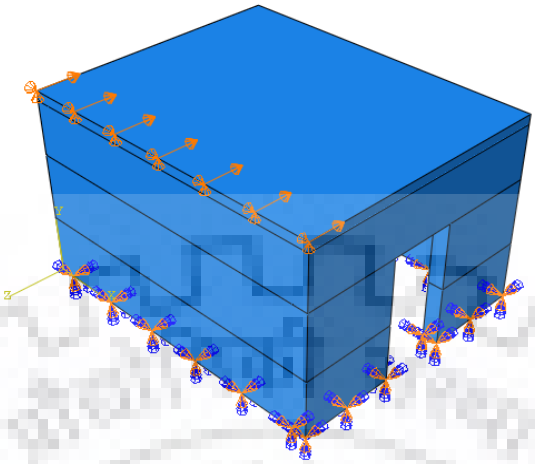

Figure 5.5 Support conditions for pushover analysis

The results in terms of stress contour and damage contour have been shown below in figures 5.6 and 5.7. The load-displacement (pushover) curve is also plotted as shown in figure 5.8.

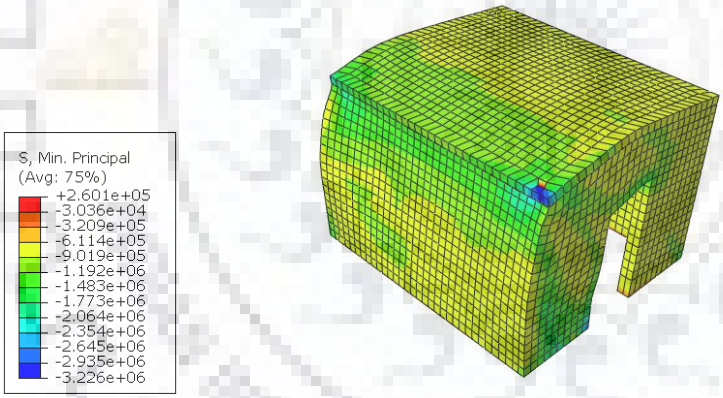

Figure 5.6 Tensile principal stress and Deformation of masonry half scale model

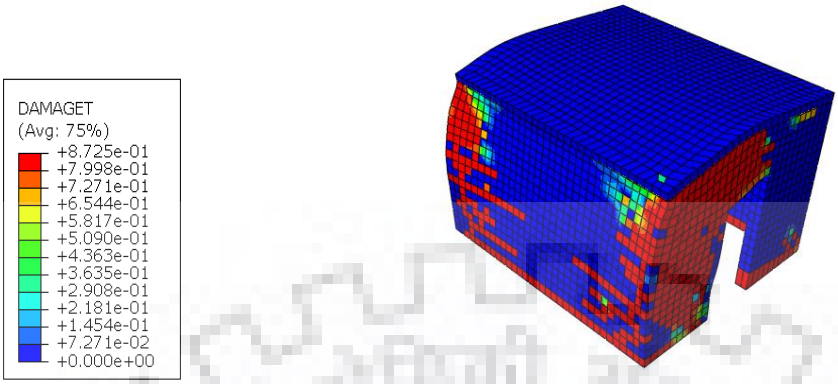

Figure 5.7 Tension damage observed in masonry half scale model

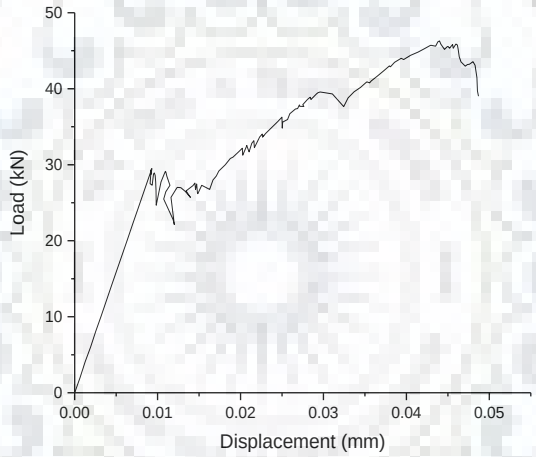

Figure 5.8 Load-displacement (pushover) curve of masonry half scale model

5.2.3 Nonlinear dynamic (Time History) analysis

Nonlinear Dynamic analysis has been performed to estimate the response of the models, subjected to recorded excitations. Nonlinear dynamic time history analysis has been done for the following acceleration time histories from figures 5.9 to 5.11 experimentally reported by Kadam (2015) recorded at the base of the half scale model. The displacement modification method of ASCE 41 (2017) is carried out to find the performance of the structure and it is found to have a performance LS.

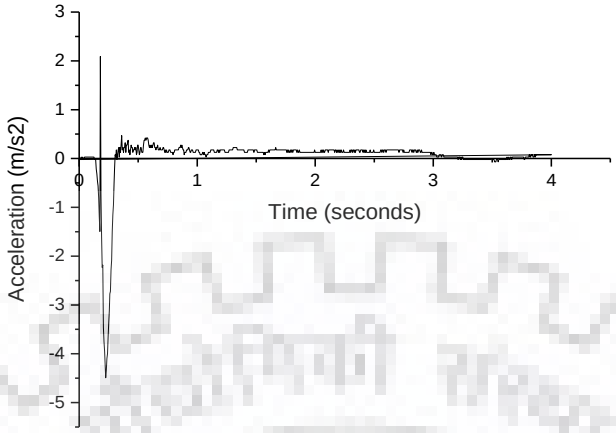

Figure 5.9 Acceleration time history recorded at the base of the model for Shock-1

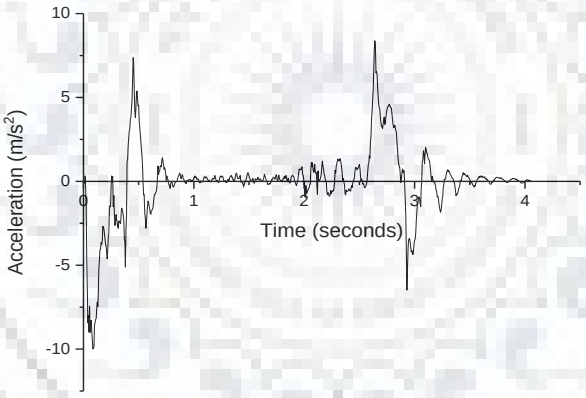

Figure 5.10 Acceleration time history recorded at the base of the model for Shock-2

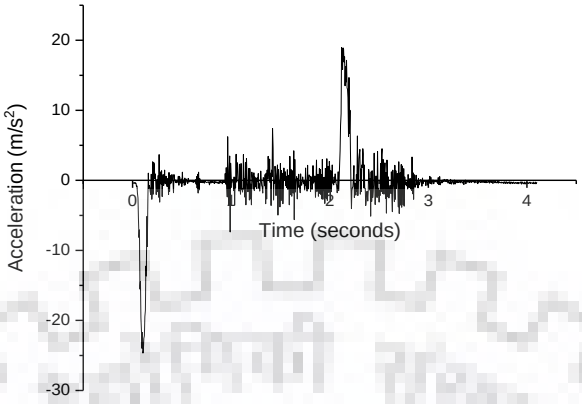

Figure 5.11 Acceleration time history recorded at the base of the model for Shock-3

The meshing for the time history analysis was the same as shown in figure 5.2. The support and loading conditions for time history analysis is shown in figure 5.12.

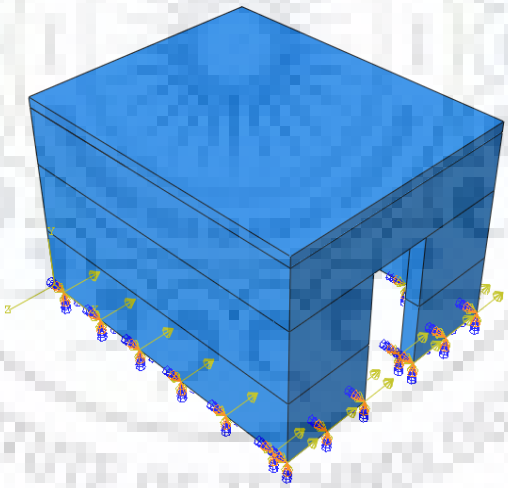

Figure 5.12 Support and loading conditions for masonry half scale model

As can be seen in figure 5.12 the acceleration time history was applied at the base of the masonry half scale model. The results of the time history analysis have been plotted in the form of a displacement-time graph as shown from figures 5.13 to 5.15

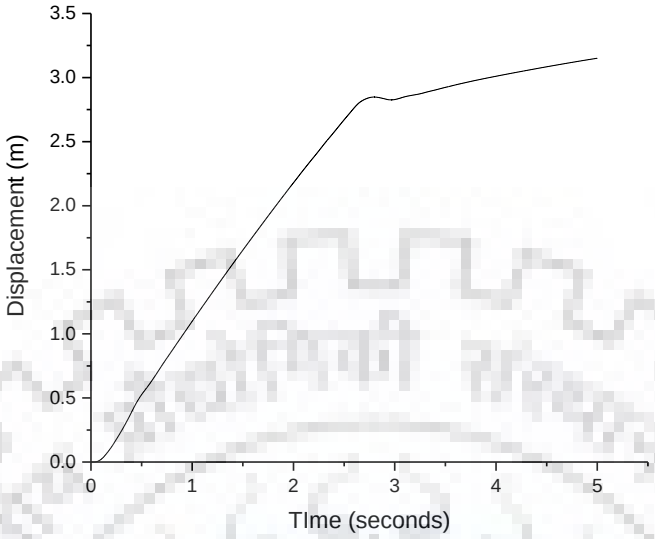

Figure 5.13 Displacement time curve for shock-1

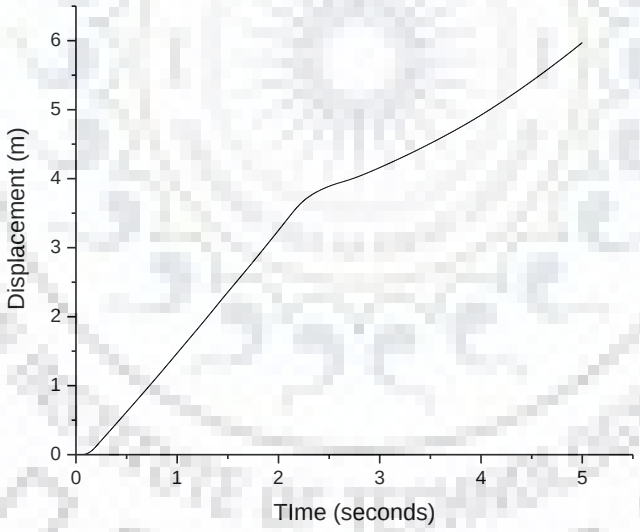

Figure 5.14 Displacement time curve for shock-2

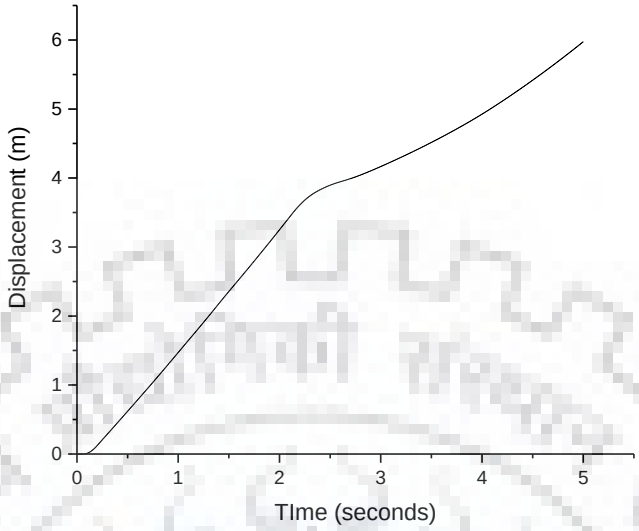

Figure 5.15 Displacement time curve for shock-2

5.3 EQUIVALENT FRAME MODELLING AND ANALYSIS

The equivalent frame modelling (EFM) is performed in SAP2000 using Dolce's criteria. The SAP2000 model is shown in figure 5.16.

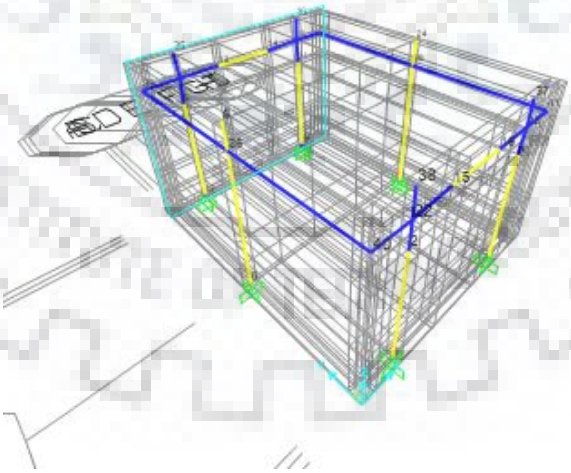

Figure 5.16 SAP2000 model

5.3.1 Modal analysis

The modal analysis in SAP2000 gave 12 modes out of which the first mode was found to be prominent with a participation factor of 0.98 and a frequency of … The first mode shape is shown in figure 5.17.

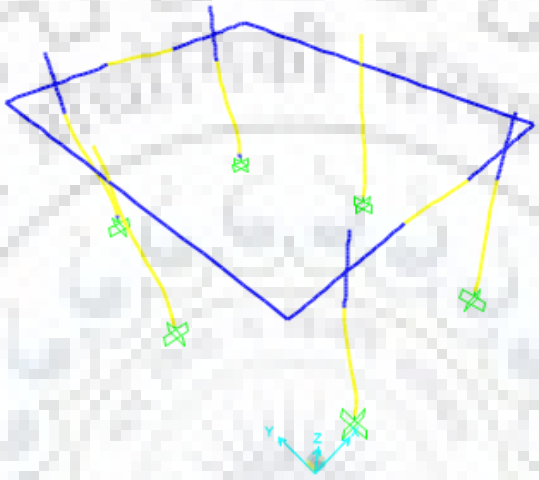

Figure 5.17 First mode shape obtained in SAP2000

5.3.2 Nonlinear Static (Pushover) analysis

Nonlinear static (pushover) analysis was performed on the half scale masonry wall in SAP2000 only in the X direction as the shock provided by the shock table was only in the X direction. The pushover curve is shown in figure 5.18. The displacement modification method of ASCE 41 (2017) is carried out to find the performance of the structure and it is found to have a performance LS.

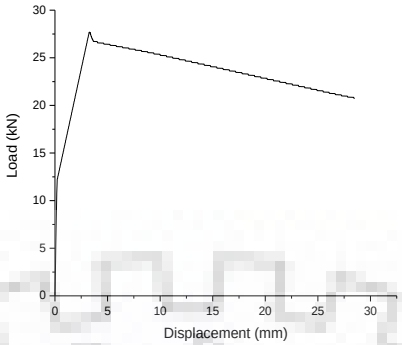

Figure 5.18 Pushover curve obtained in SAP2000

5.3.3 Nonlinear Dynamic (Time History) analysis

Nonlinear dynamic (time history) analysis was performed in SAP2000 for the same three acceleration time histories shown in figures 5.9 to 5.11. The results have been plotted as displacement-time curves as shown in figures 5.19 to 5.21. The hinge patterns in the three different shocks are shown in figure 5.22.

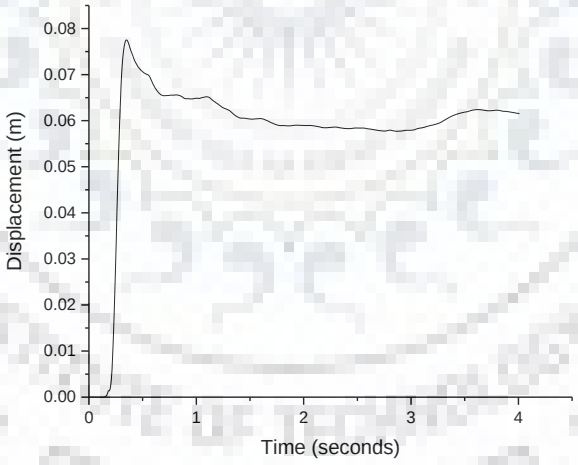

Figure 5.19 Displacement time curve for shock-1

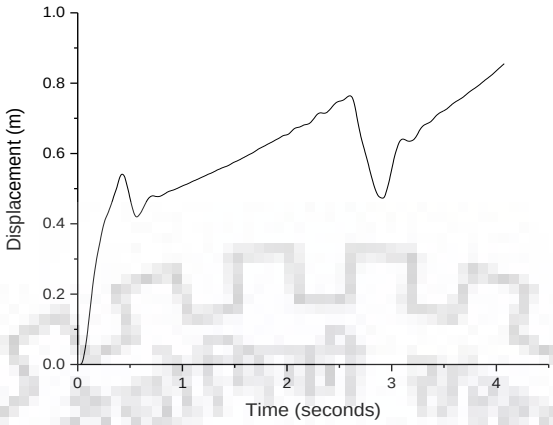

Figure 5.20 Displacement time curve for shock-2

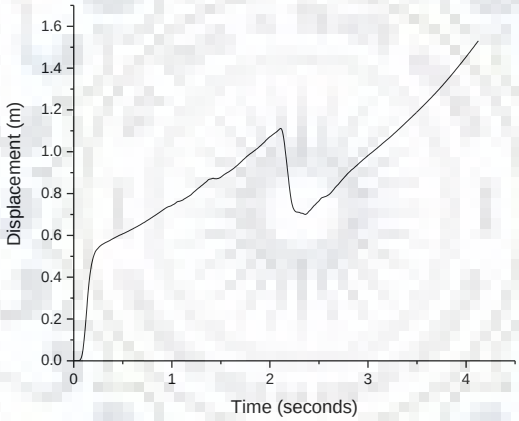

Figure 5.21 Displacement time curve for shock-3

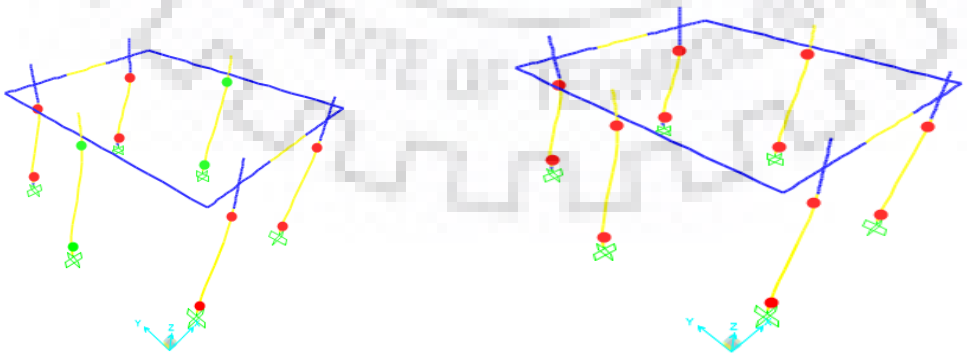

(a) (b)

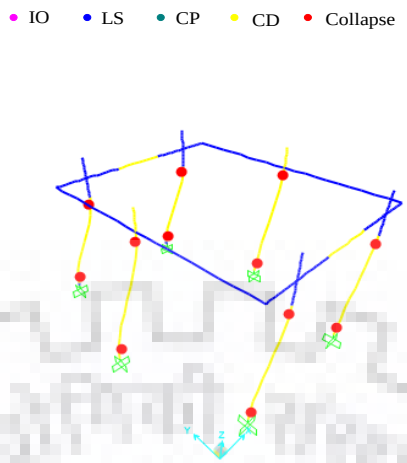

Figure 5.22 Hinge pattern in (a) Shock-1 (b) Shock-2 (c) Shock-3

5.4 RESULTS AND DISCUSSION

The results of the analysis of the half scale masonry building performed in ABAQUS and SAP2000 has been compared.

5.4.1 Comparison of modal analysis

Both softwares gave the first mode as the prominent mode of vibration however the frequency values did not match and neither did the base shear values. The frequency value observed in SAP2000 for the first mode is…. while in ABAQUS is…. The base shear observed in ABAQUS is….. while in SAP2000 the base shear observed is… The reason for this is the incorrect simulation using the EFM method in SAP2000. As the EFM method idealizes the masonry walls into frame elements it is not that accurate in predicting the results.

5.4.2 Comparison of pushover analysis

The pushover curves also did not match in both the softwares. The reason being that the tensile strength parameter reported by Kadam (2015) was not accurate. The results have been compared in figure 5.23.

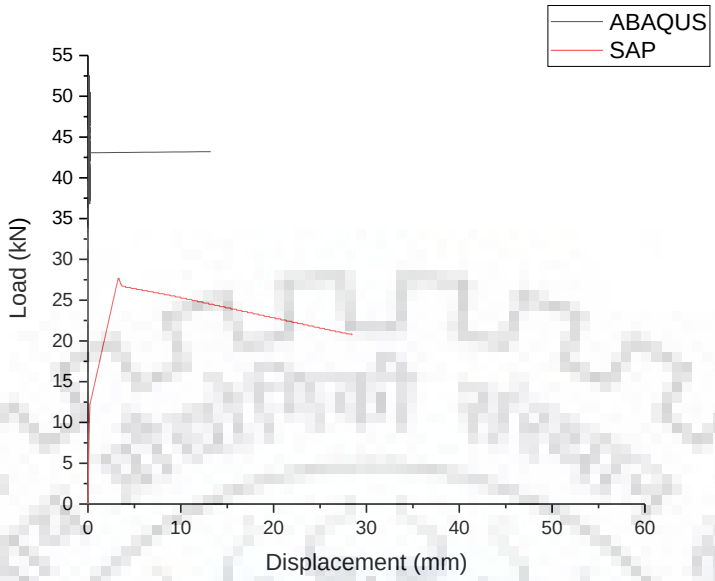

Figure 5.23 Comparison of pushover curves

5.4.3 Comparison of time history analysis

The time history analysis results being nonlinear also did not match due to the same reason of the tensile strength parameter not being reported correctly which led to inaccurate nonlinear modelling in ABAQUS. The results have been compared below in figure 5.24.

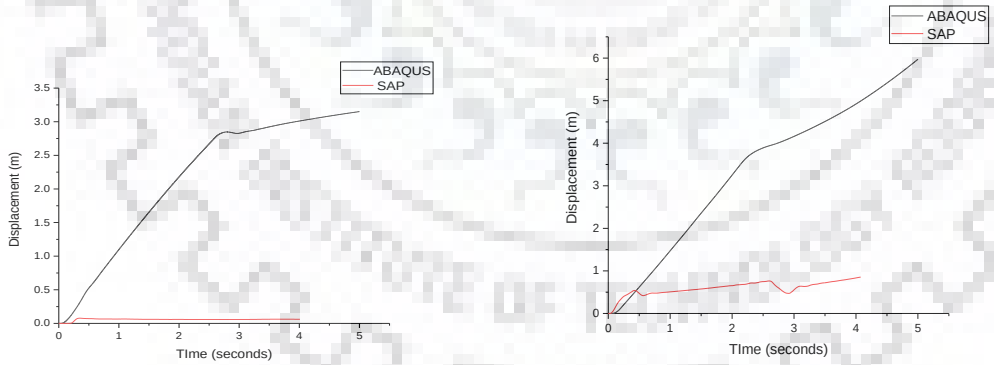

(a) (b)

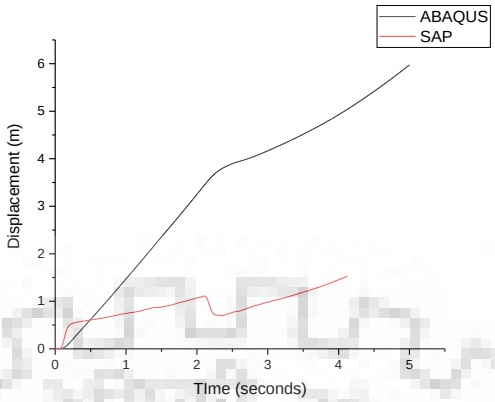

(c)

Figure 5.24 Comparison of time history results in SAP2000 and ABAQUS (a) Shock-1 (b) Shock-2 (c) Shock-3

Chapter 6

Conclusions

In this study masonry has been numerically modelled at both the component level using CDP modelling and at the global level using EFM. The numerical investigations at the component level were first carried out for the small scale test viz. the in-plane diagonal test and the out-of-plane four point bending test. The results are discussed as ahead:

6.1 BEHAVIOR OF URM COMPONENTS

The URM components modelled in ABAQUS did not match with their corresponding experimental values. The reason for this was investigated by manipulating all the CDP parameters and boundary conditions and the reason was found to be the tensile strength parameter the manipulation of which causes drastic changes in the output results. Due to this it can be inferred that the tensile strength was not reported accurately in the experiment performed by Kadam (2015). The results for the in-plane diagonal test were compared in terms of the shear stress shear strain curves and the curve obtained in the numerical analysis did not match with the experimental values. The results for the out-of-plane four point bending test were compared in terms of the load-displacement curves and it was observed that the numerical results did not match the experimental values.

6.2 BEHAVIOR OF RETROFITTED SPECIMENS

The retrofitted specimens were found to have higher strengths as due the presence of the WWM reinforcement which provided a higher ductility. However, the URM components modelled in ABAQUS did not match with their corresponding experimental values. The reason was found to be the same as for the URM components i.e. the tensile strength parameter was not reported accurately. However the numerical model was able to show that the damage occurred primarily in tension. The results for in-plane test were plotted in terms of shear stress shear strain curves and the numerical values did not match the experimental

values. The results for the out-of-plane test were plotted in terms of load-displacement curves and the numerical values did not match the experimental values.

6.3 FE MODELLING AND EFM MODELLING OF HALF SCALE MASONRY MODEL

Both the FE model and EFM model produced results that did not match the experimental values for the time history analysis. The displacement-time graph obtained in both analyses did not match the experimentally recorded values. The reason being that the experimental recording might not have been accurate or there might have been some inaccuracy in the modelling procedure. Both the models showed that the first mode was prominent but they gave different values of base shear and different values of fundamental frequency. The nonlinear data did not match in both methods which was expected due to earlier evidence of inaccuracy in reporting the tensile strength parameter.

In the present study extensive numerical analysis has been carried out for masonry components and a masonry half scale model. The results were inconclusive as the numerical results in the FE model as well as the EFM model did not match the experimental results or with each other.

REFERENCES

1. Abrams, D., Smith, T., Lynch, J., and Franklin, S. (2007). "Effectiveness of Rehabilitation on Seismic Behavior of Masonry Piers." Journal of Structural Engineering, 133(1), 32-43.

2. Abrams, D. P., "Strength and behavior of unreinforced masonry elements," 10th WCEE, Madrid, Spain, pp. 3,475-3,480, 1992.

3. Abrams, D. and Shah, N., "Cyclic Load Testing of Unreinforced Masonry Walls," Report No. 92-26-10, Advanced Construction Technology Center, Newmark Civil Engineering Laboratory, University of Illinois at Urbana-Champaign, USA, 1992.

4. Anthoine, A., Magonette G., and Magenes G. (1994), "Shear-Compression Testing and Analysis of Brick Masonry Walls," 10th ECEE, Vienna, Austria, 1657-1662.

5. Anthoine, A., Magonette G., and Magenes G. (1994), "Shear-Compression Testing and Analysis of Brick Masonry Walls," 10th ECEE, Vienna, Austria, 1657-1662.

6. Agnihotri, P., Singhal, V., and Rai, D. C. (2013). "Effect of in-plane damage on out-of-plane strength of unreinforced masonry walls." Engineering Structures, 57(0), 1-11.

7. Asteris P.G, and Tzamtzis A.D.(2002) "Non-Linear Analysis of Masonry Shear Walls, ." Proc., 6th International Masonry Conference (6thIMC), pp.493-497.

8. Azam , M. (2011). "Seismic Retrofitting of Unreinforced Masonry Buildings." M.Tech Dissertation, Indian Institute of Technology,Roorkee, Roorkee.

9. Berto, L., Saetta, A., Scotta, R., and Vitaliani, R. (2004). "Shear behavior of masonry panel: parametric FE analyses." International Journal of Solids and Structures, 41(16–17), 4383-4405.

10. Betti, M., and Vignoli, A. (2008). "Modelling and analysis of a Romanesque church under earthquake loading: Assessment of seismic resistance." Engineering Structures, 30(2), 352-367.

11. ASCE 41-17. Seismic Rehabilitation of Existing Buildings. American Society of Civil Engineers, Virginia, USA. , 2017.

12. Calvi, G. M., Kingsley, G. R., and Magenes, G. (1996). "Testing of Masonry Structures for Seismic Assessment." Earthquake Spectra, 12(1), 145-162

13. Chaimoon, K., and Attard, M. M. (2007). "Modeling of unreinforced masonry walls under shear and compression." Engineering Structures, 29(9), 2056-2068.

14. Chaimoon, K., and Attard, M. M. (2009). "Experimental and numerical investigation of masonry under three-point bending." Engineering Structures, 31(1), 103-112.

15. Chen, Y., Ashour, A. F., and Garrity, S. W. (2008). "Moment/thrust interaction diagrams for reinforced masonry sections." Construction and Building Materials, 22(5), 763-770

16. Dhanasekar, M., and Haider, W. (2008). "Explicit finite element analysis of lightly reinforced masonry shear walls." Computers & Structures, 86(1-2), 15-26.

17. Dhanasekar, M., Kleeman, P. W., and Page, A. W. (1985). "Biaxial Stress- Strain Relations for Brick Masonry." Journal of Structural Engineering- ASCE, 111(5), 1085-1100.

18. Dialer, C. (1992)" A Distinct Element Approach for the Deformation Behaviour of Shear Stressed Masonry Panels". 6th Canadian Masonry Symposium, at Saskatchewan, Canada, 765 776.

19. Dizhur, D., and Ingham, J. M. (2013). "Diagonal tension strength of vintage unreinforced clay brick masonry wall panels." Construction and Building Materials, 43(0), 418-427

20. Doherty K, Griffith MC, Lam N, Wilson J.(2002) "Displacement-based seismic analysis for out-of-plane bending of unreinforced masonry walls. Earthquake Engineering & Structural Dynamics.;31(4):833-50.

21. Dolce, M. (1989). "Models for in-plane loading of masonry walls." (Quoted in Magenes and Della Fontana, 1998).

22.Drysdale RG, Hamid AA, Baker LR.(1999) "Masonry structures: behavior and design: The Masonry Society".

23. Epperson, G. and Abrams, D., "*Nondestructive Evaluation of Masonry Buildings*,"ACTC No. 89-26-03, USA, 1989.

24. Faria, R., Oliver, J., and Cervera, M. (1998). "A strain-based plastic viscous-damage model for massive concrete structures." International Journal of Solids and Structures, 35(14), 1533-1558.

25. FEMA 356 (2000). "Prestandard and Commentary for the Seismic Rehabilitation of Buildings."Federal Emergency Management Agency, Washington, D.C., USA.

26. Ghiassi, B. (2009). "Homogenization and development of constitutive models for seismic evaluation of brick masonry structures retrofitted with reinforced concrete layer." M.Sc., Tarbiat Modares Univ., Tehran, Iran

27. Giamundo, V., Sarhosis, V., Lignola, G. P., Sheng, Y., and Manfredi, G. (2014). "Evaluation of different computational modelling strategies for the analysis of low strength masonry structures." Engineering Structures, 73(0), 160-169.

28. Kadam, S. (2015). "Seismic Evaluation and Retrofit of Masonry Buildings." Ph.D Thesis., Indian Institute of Technology Roorkee, Roorkee.

28. König, G., Mann, W., and Ötes, A., "Experimental investigation on the behavior of unreinforced masonry walls under seismically induced loads and lessons derived." 9th World Conference on Earthquake Engineering, Tokyo-Kyoto, Japan, pp. 1117-1122, 1988.

29. Lourenco, P. B., and Rots, J. G. (1997). "Multisurface interface model for analysis of masonry structures." Journal of Engineering Mechanics-ASCE, 123(7), 660-668.

30. Magenes G. and Calvi G. M., "*Cyclic Behavior of Brick Masonry Walls*," 10th World Conference on Earthquake Engineering, Madrid, Spain, pp. 3,517-3,522, 1992.

31. Magenes G. and Calvi G. M., "*Shaking Table Tests on Brick Masonry Walls*," 10th European Conference on Earthquake Engineering, Vienna, Austria , pp. 2,419-2,424, 1994.

32. Masood, A. (2006). "Out of Plane Behaviour of Unreinforced Masonry Infill Panels." Ph.D Thesis., Indian Institute of Technology Roorkee, Roorkee.

33. Morandi, P. (2006). New Proposals for Simplified Seismic Design of Masonry Buildings. *PhD Thesis*, Rose School, University of Pavia, Italy.

34. Sarangapani, G., Reddy, V., and Jagadish, K. S. (2002). "Structural characteristics of bricks, mortars and masonry." Journal of Structural Engineering (India), 29(2), 101-107.

35. Tomazevic, M., "Earthquake-Resistant Design of Masonry Buildings," Imperial College Press, London, England, 1999.

36. Vaculik, J., Griffith, M., Magenes, G., Collapse load predictions for masonry walls in bending, Proceedings of the 8th International Masonry Conference, pp. 1243-1252, Dresden, 2010.

37. Yi, T., Moon, F.L., Leon, R.T., Kahn, L.F., Progress report: Large-scale tests of low-rise unreinforced masonry building system, Georgia Institute of Technology, Department of Civil and Environmental Engineering, Atlanta, 2002.

38. Zilch, K., Schermer, D. and Scheufler, W., "Simulated Earthquake Behavior of Unreinforced Masonry Walls," 4th International PhD Symposium, Munich, Germany, 2002.